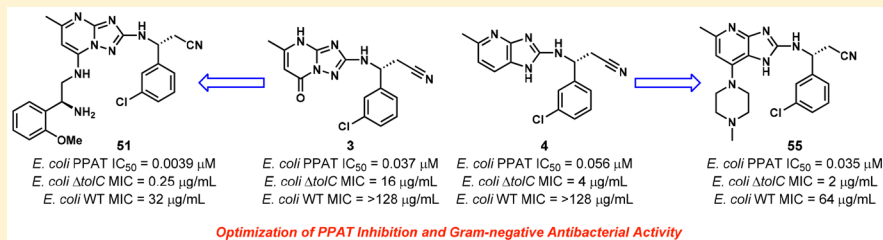


Discovery and Optimization of Phosphopantetheine Adenylyltransferase Inhibitors with Gram-Negative Antibacterial Activity

Colin K. Skepper,*^{1D} Robert J. Moreau,^{1D} Brent A. Appleton, Bret M. Benton, Joseph E. Drumm, III, Brian Y. Feng,^{1D} Mei Geng, Cheng Hu, Cindy Li, Andreas Lingel,^{1D} Yipin Lu, Mulugeta Mamo, Wosenu Mergo, Mina Mostafavi, Christopher M. Rath, Micah Steffek, Kenneth T. Takeoka, Kyoko Uehara, Lisha Wang, Jun-Rong Wei, Lili Xie, Wenjian Xu, Qiong Zhang, and Javier de Vicente

Novartis Institutes for Biomedical Research, 5300 Chiron Way, Emeryville, California 94608, United States

Supporting Information



ABSTRACT: In the preceding manuscript [Moreau et al. 2018, [10.1021/acs.jmedchem.7b01691](https://doi.org/10.1021/acs.jmedchem.7b01691)] we described a successful fragment-based lead discovery (FBLD) strategy for discovery of bacterial phosphopantetheine adenylyltransferase inhibitors (PPAT, CoAD). Following several rounds of optimization two promising lead compounds were identified: triazolopyrimidinone 3 and 4-azabenzimidazole 4. Here we disclose our efforts to further optimize these two leads for on-target potency and Gram-negative cellular activity. Enabled by a robust X-ray crystallography system, our structure-based inhibitor design approach delivered compounds with biochemical potencies 4–5 orders of magnitude greater than their respective fragment starting points. Additional optimization was guided by observations on bacterial permeability and physicochemical properties, which ultimately led to the identification of PPAT inhibitors with cellular activity against wild-type *E. coli*.

INTRODUCTION

Antibiotics have been a foundational component of medical practices since the 1940s. The steady spread of resistance, however, threatens to undermine the continued use of many traditional antibiotic classes and may eventually erode the medical advances that these drugs have made possible.^{1,2} This issue is compounded by the fact that the rate of discovery of new antibiotics has been declining for decades.³ Even as the World Health Organization (WHO), Centers for Disease Control and Prevention (CDC), and others sound the alarm over an impending “postantibiotic era”, the majority of drugs in clinical use today still belong to structural classes that were discovered during the middle of the last century.⁴

There is an especially urgent need for new antibiotics that target multidrug-resistant (MDR) and pandrug-resistant (PDR) Gram-negative bacteria, including those identified in the ESKAPE family (i.e., *Klebsiella pneumoniae*, *Acinetobacter baumannii*, *Pseudomonas aeruginosa*, and *Enterobacter spp.*).^{3c} Diverse resistance mechanisms have been described that negate the efficacy of all classes of drugs used to treat infections caused by these pathogens,⁵ including colistin, which is widely regarded as the antibiotic of last resort.⁶ Bacteria that possess

multiple resistance determinants can cause infections that are virtually untreatable.⁷

Despite high unmet medical need and decades of research in the field, the discovery of new agents to treat Gram-negative infections is challenging. This is due, in part, to the fact that Gram-negative bacteria present significant barriers to entry for small molecule drugs. These barriers include two cell membranes with opposing requirements for permeation and an array of efflux pumps with broad substrate recognition.⁸ It has been recognized that compounds with physicochemical properties suitable for Gram-negative cell entry are not well represented in corporate screening decks. Thus, it has historically been challenging to translate hits from high-throughput screens against Gram-negative bacterial targets into leads with whole-cell activity suitable for further development.⁹

One successful strategy to mitigate the challenges associated with antibacterial drug discovery is the modification of existing antibiotic scaffolds. While this approach has provided many of the drugs in use today,³ addressing the long-term need for

Received: December 15, 2017

Published: March 18, 2018



effective antibiotics will require that it be complemented by development of compounds that inhibit novel targets. One such target that has received attention recently is phosphopantetheine adenyllyltransferase (PPAT, also known as CoaD). PPAT is a hexameric enzyme that catalyzes the penultimate step in coenzyme A (CoA) biosynthesis. Coenzyme A is the universal acyl chain carrier required for many metabolic processes including the citric acid cycle and fatty acid biosynthesis.¹⁰ In bacteria, CoA is a critical cofactor in the biogenesis of membrane lipids, peptidoglycan, teichoic acids (in Gram-positive organisms), and Lipid A (in Gram-negative organisms).^{11,12} CoA is synthesized in five steps starting from pantothenic acid (vitamin B5, Figure 1).¹³ PPAT catalyzes the

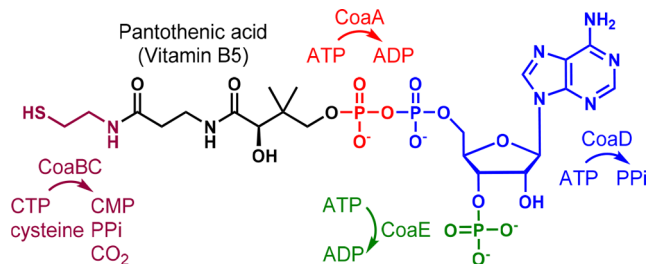


Figure 1. Schematic representation of coenzyme A biosynthesis.

fourth step in the sequence in which an adenosine monophosphate unit derived from ATP is appended to 4'-phosphopantetheine via a diphosphate ester linkage with the concomitant expulsion of inorganic pyrophosphate.¹⁴ PPAT is essential for bacterial growth and exhibits high sequence homology between species, but it shares relatively little sequence homology with the human ortholog, making it an attractive target for antibacterial drug development.^{15,16}

Several small molecule inhibitors of bacterial PPAT have been described previously,¹⁷ including two compounds from AstraZeneca (**1**, **2**) that demonstrated *in vitro* and *in vivo* inhibition of Gram-positive bacterial growth (Figure 2).¹⁸ In the previous manuscript we detailed our own efforts to identify inhibitors of Gram-negative bacterial PPAT using an FBBL approach.¹⁹ All fragment hits were found to bind at the 4'

phosphopantetheine site of *E. coli* PPAT. After several rounds of hit-to-lead optimization we identified lead compounds **3** and **4**, which exhibited nanomolar IC₅₀ values in our biochemical assay and displayed modest cellular activity against *E. coli* ΔtolC. Below we describe further optimization of this series to deliver picomolar inhibitors of PPAT from Gram-negative bacteria that demonstrate growth inhibitory activity against WT *E. coli*.

RESULTS AND DISCUSSION

As described in the preceding manuscript¹⁹ triazolopyrimidinone **3** efficiently inhibited *E. coli* PPAT and displayed modest cellular potency against the efflux-deficient *E. coli* ΔtolC mutant strain (Figure 2). Compound **3** also exhibited physicochemical properties in line with expectations for a potential Gram-negative antibiotic. An X-ray cocrystal structure with *E. coli* PPAT revealed that **3** is anchored in the pantetheine pocket of the enzyme by five direct or water-mediated hydrogen bonds (Figure 3). Specifically, the triazolopyrimidinone core interacts directly with the NH of M74 and the backbone carbonyl of D72 and through a water molecule with the NH of A75 and the side chain carbonyl of N106. The benzylic cyanomethyl forms an additional backbone interaction with the NH of S39. In an effort to further improve potency, we sought to leverage the information gained from the 39 fragment-bound X-ray cocrystal structures of *E. coli* PPAT that were obtained during our FBBL efforts. Of particular interest was the binding mode of methoxytryptamine derivative **5**, which was shown to partially overlap with **3** but was distinct in that the M74 and L102 side chains were displaced and a hydrogen bond was established between the amide NH₂ of the N106 side chain and the methoxy group of the ligand (Figure 3). In fact, ten other fragments were observed to have similar binding modes suggesting that this region of the pantetheine pocket represented a binding “hot spot”²⁰ that could be exploited to improve the affinity of compound **3**.

Given the spatial relationship between triazolopyrimidinone **3** and tryptamine **5** in the binding pocket, a series of compounds was designed and synthesized that merged the structural features of the two inhibitors. We found that phenyl

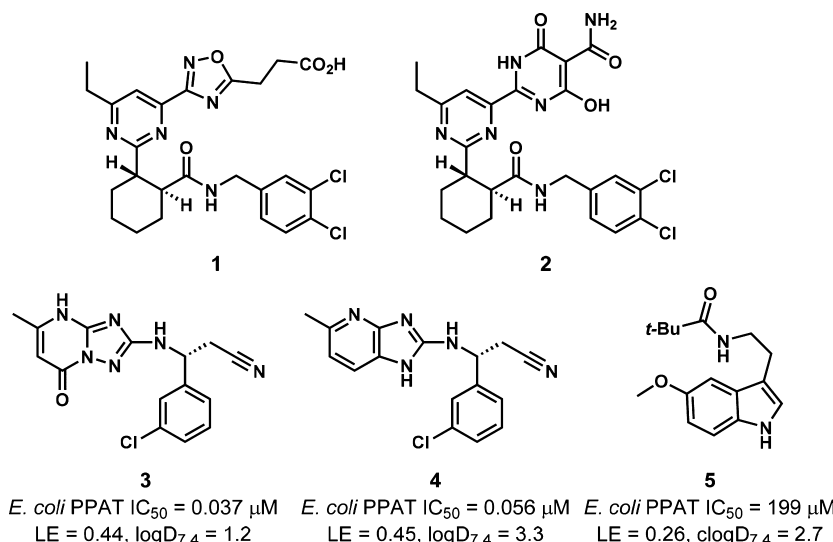


Figure 2. Structures of known bacterial PPAT inhibitors from AstraZeneca (**1**, **2**), lead compounds (**3**, **4**), and fragment hit **5**. Biochemical potency, ligand efficiency (LE), and (c)logD_{7.4} shown for compounds **3–5**.

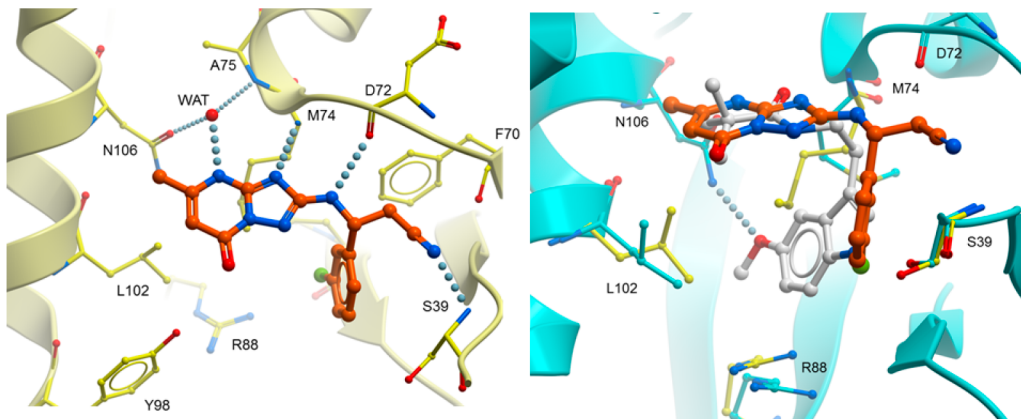


Figure 3. **Left.** X-ray crystal structure of compound 3 bound to PPAT. PPAT protein is represented as a yellow ribbon with key binding site residues displayed as yellow ball-and-stick models. Compound 3 is displayed as an orange ball-and-stick model. The key binding site water molecule is shown as a red sphere. Hydrogen bonds are displayed as light blue dotted lines. **Right.** Overlay of the crystal structure of PPAT in complex with 3 and the crystal structure of PPAT in complex with 5. PPAT in the PPAT-5 complex is represented as a cyan ribbon with key binding site residues displayed as cyan ball-and-stick models. Key binding site residues in the PPAT-3 complex are shown as yellow ball-and-stick models. Compounds 3 and 5 are shown as ball-and-stick models with 3 in orange and 5 in white. The key binding site water molecule is shown as a red sphere. Hydrogen bonds are displayed as light blue dotted lines.

Table 1. Biochemical, SPR, and MIC Data of Triazolopyrimidinones 3 and 6–9^a

Cmpd	R ¹	R ²	E. coli PPAT IC ₅₀ (nM)	E. coli PPAT SPR K _D (nM)	P. aeruginosa PPAT IC ₅₀ (nM)	E. coli ΔtolC MIC (μg/mL)	logD _{7.4}
3	CH ₂ CN	Cl	37	9.0	49	16	1.2
6	CH ₃	Cl	251	174	969	>128	1.1
7	CH ₃		167	NT	567	64	NT
8	CH ₂ CN		12	5.6	16	2	2.0
9	CH ₂ CN		13	11	11	8	0.64

^aNT = not tested.

ether 7 inhibited enzymatic activity at a level comparable to parent analog 6 and displayed weak cellular activity against *E. coli* ΔtolC (Table 1). The X-ray cocrystal structure of 7 with *E. coli* PPAT verified that the triazolopyrimidinone core was able to maintain the network of hydrogen bonds observed for 3 and that the side chains of M74 and L102 had enveloped the anisole moiety (Figure 4). However, it was also clear that the interaction with N106 could be further optimized. We expected that a carbonyl-based hydrogen bond acceptor would exhibit more favorable alignment relative to the side chain of N106 and that reinstallation of the benzylic cyanomethyl would further

enhance potency. This was indeed the case as methyl benzoate 8 exhibited a 3-fold improvement in enzymatic inhibition and an 8-fold improvement in cellular activity against *E. coli* ΔtolC relative to parent compound 3. We subsequently discovered that the distal phenyl ring of 8 could be replaced with a saturated heterocycle to provide piperidine 9. This modification lowered the measured logD_{7.4} by nearly 1.4 units and improved the solubility >40-fold while maintaining biochemical potency. The potency of compounds 8 and 9 approached the lower limit of our enzymatic assay ([PPAT] = 24 nM), and for such compounds we frequently turned to surface plasmon resonance

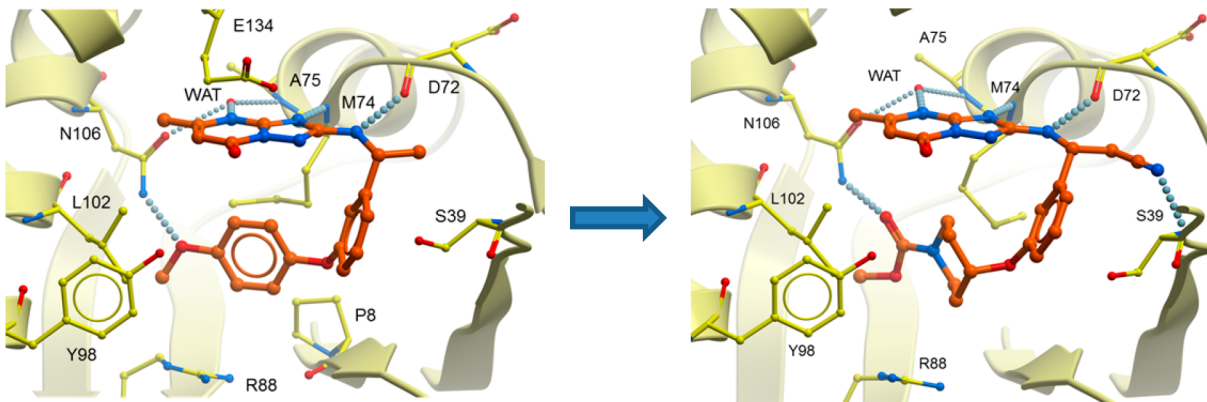


Figure 4. X-ray cocrystal structures of **7** and **9** bound to PPAT from *E. coli*. PPAT is represented as a yellow ribbon with key binding site residues displayed as yellow ball-and-stick models. Compounds are displayed as orange ball-and-stick models. The key binding site water molecule is shown as a red sphere. Hydrogen bonds are displayed as light blue dotted lines.

(SPR) to generate binding affinity data. In the case of **8** and **9** we did not observe a significant discrepancy between biochemical IC_{50} and SPR K_D ; however, this was not true of all potent compounds (*vide infra*).

Despite improvements in $\log D_{7.4}$ and biochemical potency, compounds bearing the triazolopyrimidinone core continued to exhibit only modest MIC values against *E. coli* $\Delta tolC$. The weakly acidic nature of the core heterocycle²¹ and high polarity of derivatives such as **9** (tPSA = 137) suggested that poor inner membrane permeability may account for the lack of cellular activity. We had previously observed that compound **4**, which features a 4-azabenzimidazole core, was capable of making interactions with the enzyme identical to those made by triazolopyrimidinone **3**.¹⁹ Furthermore, **4** exhibited improved cellular activity against *E. coli* $\Delta tolC$ relative to **3**, possibly as a result of superior permeability. To probe the generality of this observation, we synthesized and tested piperidine ether **10** (Table 2). We were pleased to find that **4** and **10** compared favorably to **3** and **9**, respectively; despite similar biochemical potencies, the 4-azabenzimidazoles displayed improved activity against *E. coli* $\Delta tolC$, albeit with somewhat higher $\log D_{7.4}$ values. With these results in hand, we set out to optimize the moiety between the terminal hydrogen bond acceptor (i.e., the carbamate) and the phenyl ring. This effort led to the identification of several potent analogs, including methylene-linked piperidine **11**. Compound **11** represents an example of a compound with potency that apparently exceeded the lower limit of detection in our biochemical assay, as indicated by SPR (K_D = 75 pM, biochemical IC_{50} = 9300 pM). Thioether **12** also displayed subnanomolar affinity for PPAT (SPR K_D = 280 pM). The X-ray cocrystal structures of compounds **9** and **11** provide a possible rationale for the remarkable binding affinity of the latter analogue relative to **10** (SPR K_D = 75 pM for **11** vs 1900 pM for **10**; no crystal structure was available for **10**). As seen in Figure 5, the core heterocycles of **9** and **11** occupy nearly identical positions and orientations. The piperidine moiety of compound **11**, however, adopts a bound conformation that is likely closer to the ground state conformation than the corresponding moiety in **9**. Specifically, the piperidine aryloxy substituent of **9** adopts an axial orientation, whereas the corresponding methylene substituent in **11** enjoys an equatorial disposition. In addition, the $\sim 90^\circ$ torsion angle between the phenyl ring, the methylene linker, and the piperidine tertiary carbon of **11** is in line with the preferred conformation for primary alkyl substituents on aryl rings. In contrast, primary

and secondary alkoxy substituents prefer to adopt a planar conformation (torsion angle $\sim 0/180^\circ$) as determined from an analysis of CSD and PDB structures.²² Finally, the methylene linker group in **11** makes lipophilic interactions with nearby residues, in particular A37, F70, and G9. In contrast, compound **10** projects an ether oxygen toward the same region of the binding pocket.

Significantly, both **11** and **12** displayed weak but measurable MIC values against WT *E. coli* (128 and 64 $\mu\text{g}/\text{mL}$, respectively). This demonstration of WT Gram-negative activity was a major milestone in the program and encouraged further exploration. More polar analogs of **12**, such as sulfone **13** and sulfonylpiperazine **14**, had comparable biochemical potency but reduced cellular activity; piperazinone **15** was markedly less active. Truncation of the piperidine ring of **10** to a pyrrolidine provided diastereomers **16** and **17**, with the preferred diastereomer (**17**) having activity similar to **10**, except for 16-fold weaker cellular activity against *E. coli* $\Delta tolC$. Replacing the linking oxygen atom with carbon provided pyrrolidines **18** and **19**, whose improved biochemical potencies were in line with previous observations in the piperidine series, with **19** displaying a measurable MIC against WT *E. coli* (64 $\mu\text{g}/\text{mL}$).

Additional insight into the SAR of this series was provided by the use of a novel, mass spectrometry (MS)-guided metabolomics assay. This assay, described in detail elsewhere,²³ was designed to measure the concentration of either free CoA-SH or acetyl CoA in bacterial cells in the presence or absence of a PPAT inhibitor. The reported IC_{50} values indicate the concentration of compound required to reduce the level of a given CoA metabolite by 50% relative to untreated control cells. Importantly, this assay allowed us to assess target engagement in efflux-competent, WT Gram-negative cells at concentrations well below those required to observe an MIC. Table 3 shows CoA-SH metabolite data for compounds **3**, **4**, **9**, and **10**.

Compound **4** proved to be slightly more potent than **3** in the *E. coli* $\Delta tolC$ metabolite assay. However, in WT *E. coli* **4** was at least 40-fold more potent than **3** (IC_{50} = 4.76 μM for **4** vs >200 μM for **3**). These data are consistent with the hypothesis that the triazolopyrimidinone core suffers from generally poor permeability as a consequence of slow permeation, efflux, or (more likely) both. This trend continued for compounds **9** and **10**, where the azabenzimidazole analog (**10**) was approximately

Table 2. Biochemical, SPR, and MIC Data for Azabenzimidazoles 4 and 10–19^a

Cmpd	R ²	<i>E. coli</i> PPAT IC ₅₀ (nM)	<i>E. coli</i> PPAT SPR <i>K</i> _D (nM)	<i>P. aeruginosa</i> PPAT IC ₅₀ (nM)	<i>E. coli</i> ΔtolC MIC (μg/mL)	<i>E. coli</i> WT MIC (μg/mL)	logD _{7.4}
4	Cl	56	10	64	4	>128	3.3
10		11	1.9	9.2	0.25	>128	3.0
11		9.3	0.075	2.5	0.125	128	2.8
12		8.2	0.28	2.7	0.06	64	3.7
13		9.3	NT	2.4	2	>128	1.9
14		26	1.1	13	32	>128	2.0
15		231	NT	488	NT	NT	1.4
16		536	NT	502	>128	>128	2.8
17		12	7.7	9.3	4	>128	2.7
18		46	NT	8.3	1	>128	3.1
19		20	NT	3.8	0.125	64	NT

^aNT = not tested.

20-fold more potent than **9** as measured by the metabolite assay in both WT and efflux-deficient *E. coli*.

Comparing the data for compounds **4** and **10**, however, illustrates one of the challenges of Gram-negative antibacterial

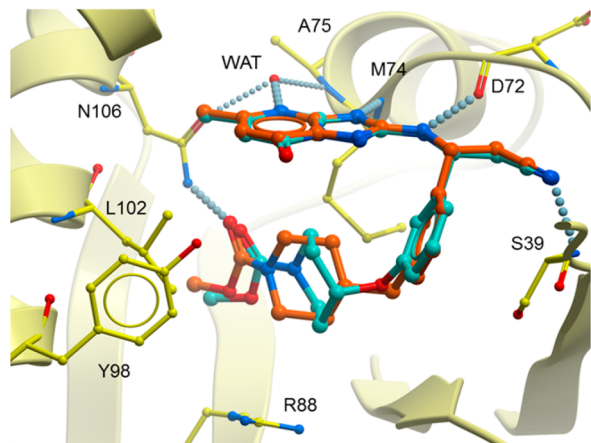


Figure 5. Overlay of X-ray cocrystal structures of **9** and **11** bound to PPAT from *E. coli*. PPAT is represented as a yellow ribbon with key binding site residues displayed as yellow ball-and-stick models. Compounds are shown as ball-and-stick models with **11** in orange and **9** in cyan. The key binding site water molecule is shown as a red sphere. Hydrogen bonds are displayed as light blue dotted lines.

drug discovery. As discussed above, compound **10** was designed to take advantage of a binding “hot spot” in the PPAT active site by engaging in a hydrogen-bonding interaction with the side chain of N106. The success of this design principle was manifested by a 5-fold improvement in biochemical potency for **10** compared to **4**. This translated to a 15-fold improvement in

metabolite inhibition and a 16-fold improvement in MIC against *E. coli* $\Delta tolC$. However, **10** was 2–3-fold less potent than **4** in the metabolite assay against WT *E. coli*. Put another way, the *E. coli* WT/ $\Delta tolC$ metabolite IC₅₀ ratio is ~13 for compound **4**, compared to ~500 for compound **10**. Thus, while the intrinsic potency of compound **4** was improved by elaboration to **10**, this came at the cost of significantly increased efflux in WT *E. coli* cells. Although further optimization of **10** provided compounds with on-scale MICs against WT *E. coli*, such as **11**, **12**, and **19**, a very large efflux shift was still evident. The identification of additional structural features that would improve both biochemical potency and Gram-negative cellular permeability and/or efflux therefore became a priority for the program.

Inspection of the X-ray cocrystal structure of **11** overlaid with that of dephospho-CoA revealed that the tertiary carbon atom of the piperidine ring of **11** offered a vector for growing toward the polar portion of the active site that accommodates the phosphate ester linkage of the enzymatic reaction product (Figure 6). We hoped that growing toward this pocket would result in formation of additional polar interactions with the protein, or even ATP, thereby providing a boost in potency without increasing (or perhaps even reducing) lipophilicity. A number of compounds were prepared to test this hypothesis (Table 4). Small, polar substituents branching from the tertiary piperidine carbon of **11** were well tolerated (**20–23**) and provided PPAT inhibitors with potency comparable to the parent compound. In addition, larger substituents including aliphatic alcohols, acids, and nitriles (**24–27**) also provided

Table 3. Comparison of Biochemical IC₅₀, Metabolite IC₅₀, and MIC Data for **3, **4**, **9**, and **10****

	<i>E. coli</i> PPAT IC ₅₀ (nM)	<i>E. coli</i> $\Delta tolC$ CoA-SH metabolite IC ₅₀ (μM)	<i>E. coli</i> WT CoA-SH metabolite IC ₅₀ (μM)	<i>E. coli</i> $\Delta tolC$ MIC (μg/mL)	<i>E. coli</i> WT MIC (μg/mL)
3					
	37	0.59	>200	16	>128
4					
	56	0.37	4.76	4	>128
9					
	13	0.45	>200	8	>128
10					
	11	0.024	11.9	0.25	>128

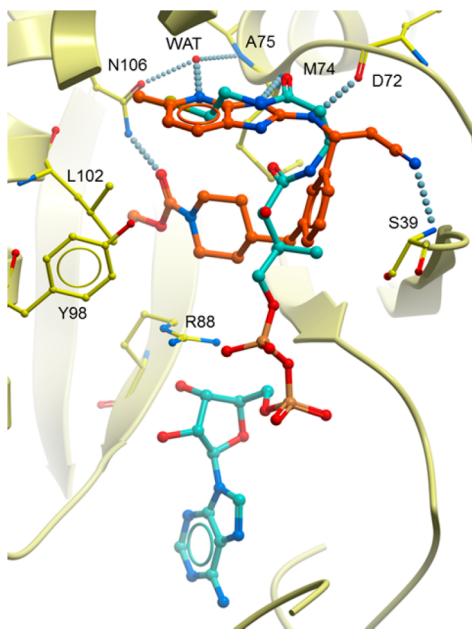


Figure 6. X-ray cocrystal structure of compound 11 bound to PPAT overlaid with the bound conformation of dephospho-CoA in its complex crystal structure with PPAT (pdb code: 1b6t). PPAT in the complex with 11 is represented as a yellow ribbon with key binding site residues displayed as yellow ball-and-stick models. Ligands are shown as ball-and-stick models with 11 in orange and dephospho-CoA in cyan. The key binding site water molecule is shown as a red sphere. Hydrogen bonds are displayed as light blue dotted lines.

potent compounds (many with pM K_D values) but failed to deliver a compound with improved activity over 11 in cellular assays. Further efforts were met with a similar lack of success, and this strategy was deprioritized.

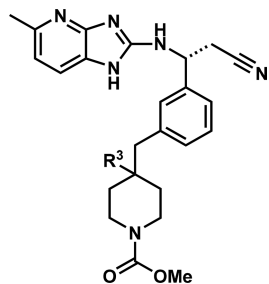
In parallel with our survey of the phosphate ester binding site, we also explored a distinct hydrophobic pocket defined by the side chains of Y98, Q101, L102, and L131 that was first identified from an X-ray cocrystal structure with HTS hit 28 (Figure 7). The triazolopyrimidinone core of compound 3 provided a convenient vector for growing toward this pocket with more advanced inhibitors, and this led to the series of triazolopyrimidines summarized in Table 5. Even without the key nitrile substituent common to the triazolopyrimidinone and azabenzimidazole series, initial compounds such as diarylamines 29 and 30 displayed strong inhibition of PPAT and potent inhibition of the growth of *E. coli* $\Delta tolC$. In the context of *N*-acetyl indoline 30, introduction of the aforementioned nitrile (31) provided at least a 2-fold improvement in biochemical and cellular potency while reducing $\log D_{7.4}$.²⁴ Aside from the expected array of hydrogen bonds between the core scaffold and protein, much of the binding affinity for these inhibitors is derived from hydrophobic interactions between the aromatic heterocycle appended to the triazolopyrimidine core and the side chains of L102, L131, and Q101, as well as $\pi-\pi$ stacking with Y98.²⁵ Expansion of the SAR revealed a preference for a two-carbon linker between the C7 amine and a pendant aromatic group; phenethylamine 32 displayed good activity that could be further enhanced by rigidifying the linker as a *trans*-substituted cyclopropane (33). Replacement of the phenyl ring of 32 with aromatic heterocycles was well tolerated and led to the identification of more polar analogues such as pyrazole 34, which was shown by X-ray crystallography to bind in the Y98 pocket and engage in a hydrogen bond with the side chain

carbonyl of Q101. While installation of the benzylic cyanomethyl again led to a marked improvement in activity (35), activity against WT *E. coli* remained elusive.

The aforementioned lipophilicity-driven binding resulted in inefficient inhibitors ($\text{LipE} \sim 1.5\text{--}2$), and it became imperative to discover new groups at C7 that could not only modulate the physicochemical properties of our inhibitors but also address our goal of identifying compounds with reduced efflux and/or improved permeability in WT Gram-negative bacteria. We began by introducing small, weakly basic amines (36–39) and found that compounds lacking the nitrile substituent (36 and 38) were relatively weak inhibitors of PPAT; however, upon introduction of the nitrile (37 and 39) a dramatic boost in potency was observed (Table 5). X-ray cocrystal structures showed that the Y98/Q101/L102 hydrophobic pocket had collapsed, as expected, and suggested that the terminal nitrogen of piperazine 36 was engaged in a hydrogen bond with the Y98 phenol. Although these compounds had only modest MIC values against *E. coli* $\Delta tolC$, consideration of metabolite inhibition data proved instructive and encouraging (Table 6).²³ While 31 demonstrated relatively potent reduction of CoA-SH levels in $\Delta tolC$ and WT *E. coli* (consistent with its biochemical potency and *E. coli* $\Delta tolC$ MIC), it suffered from a high $\log D_{7.4}$ and negligible solubility. The pyrazole analog 35 was somewhat improved in this regard, but piperazine 37 displayed an intriguing profile. Despite modest intrinsic potency, 37 demonstrated robust inhibition of CoA-SH formation in the metabolite assay against WT *E. coli* cells, as well as a more favorable $\log D_{7.4}$ and much improved solubility. Clearly, this warranted further exploration.

In an attempt to capitalize on these new discoveries, we hypothesized that the combination of a weakly basic amine with a substituent capable of engaging in a $\pi-\pi$ stacking interaction with Y98 would improve both Gram-negative bacterial permeation and intrinsic potency, respectively. Guided by the wealth of structural information we had accumulated, we synthesized S benzylamine 40 and were gratified to find that it prevented the growth of WT *E. coli* at concentrations as low as 32 $\mu\text{g}/\text{mL}$ (Table 7). Further, the poor inhibitory activity of diastereomer 41 and alcohol 42, particularly in cellular assays, helped support our hypothesis that an appropriately substituted amine could increase potency and confer improved permeability against WT *E. coli*. Close-in SAR showed that substitution of the amine or the linker ablated both biochemical and cellular potency (data not shown), but thiophenes (43–44) and fluorophenyl analogs (45–47) were well tolerated and expanded the number of compounds with activity against WT *E. coli*. Unfortunately, replacement of the phenyl ring with the more polar pyridine ring (48–50) proved deleterious to cellular activity. The data for the fluorophenyl and pyridyl series of compounds were suggestive of improved cellular activity with proximity between the hydrogen bond acceptor and the amine. Our hypothesis was that this arrangement might allow for an internal hydrogen bond that could improve inner-membrane permeability. As a result, we synthesized *o*-methoxyphenyl compound 51. This analog was the most potent compound of the series, and it bound to the enzyme in a manner consistent with previous observations (Figure 8). Unfortunately, further optimization of this example was unsuccessful, as were parallel efforts to reduce the lipophilicity, such as by replacing the phenyl ring with a cyclopropane (52) or 5-membered heteroaromatic groups (53–54).

Table 4. Biochemical, SPR, and MIC Data of Imidazolopyridines 20–27^a



^aNT = not tested.

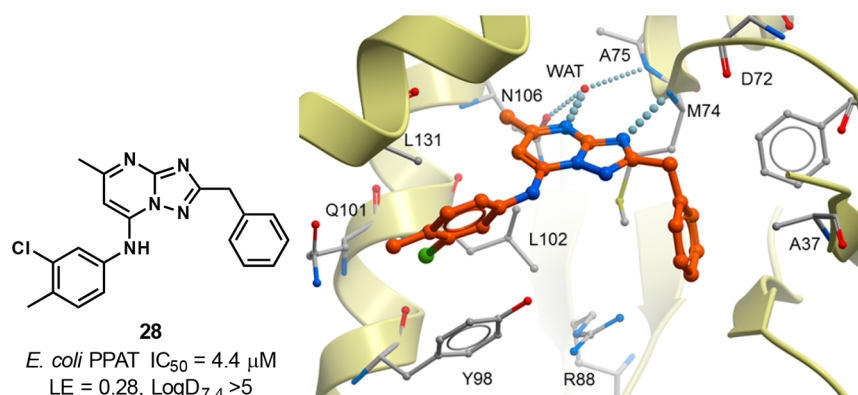
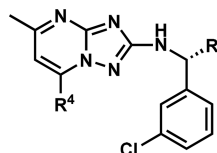


Figure 7. X-ray cocrystal structure of **28** bound to PPAT from *E. coli*. PPAT protein is represented as a yellow ribbon with key binding site residues displayed as gray ball-and-stick models. Ligand is shown as an orange ball-and-stick model. The key binding site water molecule is shown as a red sphere. Hydrogen bonds are displayed as light blue dotted lines.

In the preceding manuscript, we described a positive correlation between on-target potency and electrostatic potential at the core heterocyclic nitrogen atoms that make direct and water-mediated hydrogen bonds with the protein.¹⁹ In addition, it was apparent that the azabenzimidazole core was associated with improved Gram-negative permeability. Combining these observations with information gleaned from the chemical series described above, we targeted compound **55**, which features a piperazine ring appended to the azabenzimi-

dazole core. We were pleased to find that this relatively compact molecule exhibited on-scale activity against WT *E. coli* comparable to **51** but with reduced molecular weight and lipophilicity. The *in vitro* profile of **55** is presented in Table 8. Remarkably, although **55** is 10-fold less potent than **51** in the biochemical assay and by SPR, **55** is only 2-fold less potent against WT *E. coli*. Given these promising data, we made a final attempt to improve the activity by hybridizing **10** and **55** to provide analog **56**. We were disappointed to find that the

Table 5. Biochemical, SPR, and MIC Data of Triazolopyrimidines 29–39^a


Cmpd	R ⁴	R ¹	E. coli PPAT IC ₅₀ (nM)	E. coli PPAT SPR K _D (nM)	P. aeruginosa PPAT IC ₅₀ (nM)	E. coli ΔtolC MIC (μg/mL)	E. coli WT MIC (μg/mL)	logD _{7.4}
29		CH ₃	14	8.8	29	1	>128	4.4
30		CH ₃	7.8	1.2	6.8	0.125	>128	4.6
31		CH ₂ CN	4.0	NT	4.3	0.06	>128	3.9
32		CH ₃	48	NT	151	4	>128	>4.8
33		CH ₃	16	6.1	34	2	>128	4.9
34		CH ₃	36	5.9	228	2	>128	2.9
35		CH ₂ CN	5.4	1.1	6.1	0.5	>128	3.8
36		CH ₃	307	NT	218	32	>128	3.3
37		CH ₂ CN	21	3.9	9.7	4	>128	2.4
38		CH ₃	270	NT	235	>128	>128	NT
39		CH ₂ CN	14	21	12	4	>128	2.8

^aNT = not tested.

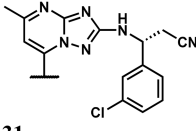
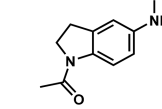
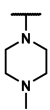
combination proved to be nonadditive, and the overall profile was similar to that of **10**. While it was recognized that an analog of compound **51** featuring the azabenzimidazole core would be an attractive target, cumulative knowledge acquired on the project to date suggested there were limited avenues for further optimization of such a compound.

Eflux pumps in Gram-negative bacteria present a notorious barrier-to-entry for small molecules.⁸ In general, our attempts to identify compounds with reduced susceptibility to efflux found limited success, suggesting that recognition by pumps might be an inherent feature of the general scaffold. Over the

course of the program we examined in excess of 20 different core structures in attempts to find alternative chemical matter with an improved profile. Only very close analogues retained activity against PPAT (e.g., 4-azabenzothiazole, compound **40** in the preceding manuscript¹⁹), and these compounds did not offer an advantage over our lead scaffolds. Compounds that featured more drastic changes to the core heterocycle usually suffered from a precipitous loss of on-target potency.

The challenge of overcoming efflux is due in part to the presence of multiple redundant pumps in the Gram-negative cell. The problem is exacerbated for cytoplasmic targets such as

Table 6. Biochemical IC₅₀, Metabolite IC₅₀, MIC, logD_{7.4}, and Solubility Data for 31, 35, and 37

	<i>E. coli</i> PPAT IC ₅₀ (nM)	<i>E. coli</i> $\Delta tolC$ CoA-SH metabolite IC ₅₀ (μ M)	<i>E. coli</i> WT CoA-SH metabolite IC ₅₀ (μ M)	<i>E. coli</i> $\Delta tolC$ MIC (μ g/mL)	<i>E. coli</i> WT MIC (μ g/mL)	logD _{7.4}	Sol. (PBS) (μ g/mL)
31							
							
	4.0	<0.006	2.4	0.06	>128	3.9	<0.6
35							
							
	5.4	0.012	74	0.5	>128	3.8	23.8
37							
							
	21	0.097	41	4	>128	2.4	>729

PPAT, as small molecule inhibitors must cross both the inner and outer membranes which impede the passage of hydrophilic and lipophilic molecules, respectively. Despite a concerted effort from many research groups, it has proven difficult to derive a set of broadly applicable “rules” based on structure or physicochemical properties that could be used to guide optimization of efflux and permeability.^{8,9} The data in Table 8 indicates that efflux is a somewhat more significant barrier to permeability for our compounds than influx through the outer membrane. This is manifested by MIC values against *E. coli* *imp4213* (an outer-membrane-deficient strain) which are uniformly higher than MICs against *E. coli* *ΔtolC* (an efflux-deficient strain). To varying degrees, the compounds in Table 8 also exhibit a shift in MIC between *E. coli* *ΔacrB*, in which the inner membrane component of a specific tripartite RND efflux pump, AcrAB-TolC, is knocked out, and *E. coli* *ΔtolC*, in which TolC, the major outer membrane channel associated with multiple transporters, is removed resulting in a severely efflux-impaired mutant.²⁶ This suggests that these compounds are recognized by multiple efflux pumps in *E. coli* in addition to AcrAB-TolC, a conclusion supported by recently published data.²³ Unsurprisingly, our compounds were also broadly impacted by efflux in *P. aeruginosa*; however, due to an absence of wild-type activity the extent of efflux is difficult to quantify.

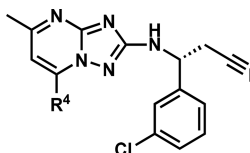
Interestingly, susceptibility to efflux in *E. coli* is not uniform across our series. The *ΔacrB/ΔtolC* shift is particularly pronounced for compounds **10** and **11** (*E. coli* *ΔacrB* MIC/*E. coli* *ΔtolC* MIC = 128 and \geq 128 fold, respectively). Compound **55** has a much smaller 4-fold shift between *E. coli* *ΔacrB* and *ΔtolC* and exhibits a relatively low overall efflux ratio of 32-fold between WT *E. coli* and *E. coli* *ΔtolC* (compared to 128-fold for **51** and at least 512-fold for **10** and **11**). This difference may be due to reduced recognition by efflux pumps on the part of **55** but may also be the result of a greater rate of influx. Indeed, **55** shows a relatively small shift between WT *E. coli* and *E. coli* *imp4213* (8-fold for **55** vs 32-fold for **51** and 64-fold for **11**).²⁷ The improved overall permeability of **55** might be derived from the combination of several key structural features: 1) The 4-azabenzimidazole core, which as described above appears to enjoy improved permeability relative to alternate cores such as triazolopyrimidinone (**3**). 2) A weakly basic amine ($pK_a = 7.4$ for **55**). Protonation of the amine may

help to drive compound influx, perhaps through interaction with outer membrane porins or the bacterial transmembrane potential. Once in the periplasm, the neutral form of the amine would be expected to diffuse readily through the inner membrane. 3) A relatively small and compact structure. Compared to **55**, compounds such as **10** and **11** are larger, feature more rotatable bonds, and have additional H-bond donors and acceptors which may serve to reduce membrane diffusion rates, increase susceptibility to efflux recognition, or both. This may explain the much larger efflux ratios observed for **10** and **11**.

■ TARGET SELECTIVITY OF PPAT INHIBITORS

In the human CoA biosynthetic pathway the role of PPAT is performed by a bifunctional enzyme called CoA synthase (CoASy), which combines the activities of PPAT and dephospho-CoA kinase (DPCK). Although CoASy does not share significant homology with bacterial PPAT, it does have similarity to bacterial dephospho-CoA kinase (CoAE).¹⁶ To assess the selectivity of our PPAT inhibitor series we constructed a strain (JWK0002) derived from *E. coli* *ΔtolC*. In this strain the bacterial CoAD enzyme was replaced by the human PPAT ortholog (*E. coli* *ΔtolC*:FRT *ΔcoaD*:*aph* (K_m^R) + pNOV016 (*Hs.coaSY*, Gm^R)). The susceptibility of JWK0002 to all tested antibiotics was similar to the parent strain (see the Supporting Information). Our PPAT inhibitors, while suppressing the growth of *E. coli* *ΔtolC*, did not affect the growth of JWK0002. This indicates that our compounds specifically target *E. coli* PPAT (CoAD) but not human PPAT (CoASy) (see Table 8 and the Supporting Information). In order to further confirm the on-target nature of **51**, *E. coli* *ΔtolC* cells resistant to the inhibitor were selected at 2-fold, 4-fold, and 8-fold the MIC. The frequency of resistant mutants under these conditions was 1.3×10^{-8} , 8×10^{-9} , and 4×10^{-9} , respectively. This frequency of resistance is similar to the fluoroquinolone gatifloxacin, which exhibited a frequency of 3.2×10^{-8} at 4-fold the MIC against a clinical strain of *E. coli*.²⁸ We sequenced the *coaD* gene from a subset of resistant mutants and identified the F70Y, A75P, and N106Y mutations in the pantetheine site that disrupt key interactions between **51** and PPAT. Specifically, the A75P and N106Y mutations disrupt the hydrogen bonding network by displacing the ordered water that engages the core

Table 7. Biochemical, SPR, and MIC Data of Triazolopyrimidines 40–54^a



40

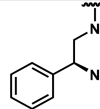
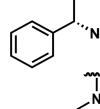
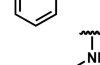
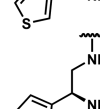
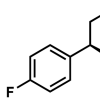
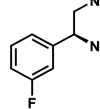
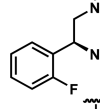
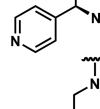
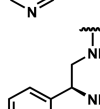
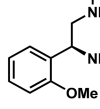
Cmpd	R ⁴	<i>E. coli</i> PPAT IC ₅₀ (nM)	<i>E. coli</i> PPAT SPR K _D (nM)	<i>P. aeruginosa</i> PPAT IC ₅₀ (nM)	<i>E. coli</i> ΔtolC MIC (μg/mL)	<i>E. coli</i> WT MIC (μg/mL)	logD _{7.4}
40		6.6	NT	4.1	0.25	32	3.4
41		46	NT	39	8	>128	3.2
42		7.0	5.5	13	0.25	>128	3.6
43		6.0	3.3	4.5	1	64	3.0
44		4.8	2.0	5.2	0.25	64	3.3
45		4.8	6.7	8.0	0.5	64	NT
46		3.7	2.9	5.4	0.25	64	3.7
47		3.4	0.46	5.0	0.125	64	3.2
48		11	6.7	14	4	>128	2.2
49		15	4.8	22	4	>128	2.3
50		11	6.5	15	2	>128	1.9
51		3.9	0.83	7.0	0.25	32	3.1

Table 7. continued

Cmpd	R ⁴	<i>E. coli</i> PPAT IC ₅₀ (nM)	<i>E. coli</i> PPAT SPR K _D (nM)	<i>P. aeruginosa</i> PPAT IC ₅₀ (nM)	<i>E. coli</i> ΔtolC MIC (μg/mL)	<i>E. coli</i> WT MIC (μg/mL)	logD _{7.4}
52		43	25	9.9	8	>128	1.3
53		12	NT	15	1	>128	NT
54		7.7	NT	10	4	>128	NT

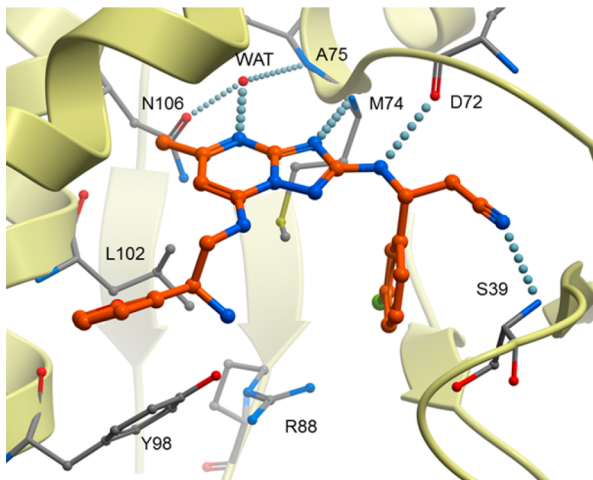
^aNT = not tested.

Figure 8. X-ray cocrystal structure of **51** bound to PPAT from *E. coli*. PPAT protein is represented as a yellow ribbon with key binding site residues displayed as gray ball-and-stick models. Ligand is shown as an orange ball-and-stick model. The key binding site water molecule is shown as a red sphere. Hydrogen bonds are displayed as light blue dotted lines.

azabenzimidazole pyridine nitrogen. The F70Y mutation, on the other hand, introduces a polar tyrosine side chain that potentially creates an unfavorable interaction with the chlorophenyl group. These mutants all displayed a loss of susceptibility to **51**; clones harboring either the F70Y or A75P mutations were 64-fold less susceptible, and the N106Y mutation resulted in a > 128-fold loss in activity. Genetically reconstructed mutant strains preserved the resistant phenotype only to PPAT inhibitors and not to other known antibiotics, demonstrating the on-target activity of our optimized inhibitors (data not shown).

■ CHEMISTRY

The synthesis of triazolopyrimidinone derivatives is outlined in **Schemes 1–3**. Compound **7** was synthesized starting from commercially available benzylamine **57**, which was converted to aminotriazole **58** by treatment with diphenyl cyanocarbonimidate followed by hydrazine hydrate (**Scheme 1**). The triazolopyrimidinone **59** was furnished in good yield via condensation with ethyl acetoacetate under microwave conditions. This compound was then reacted with 4-

methoxyphenol under Chan-Lam-Evans conditions²⁹ to provide **7**.

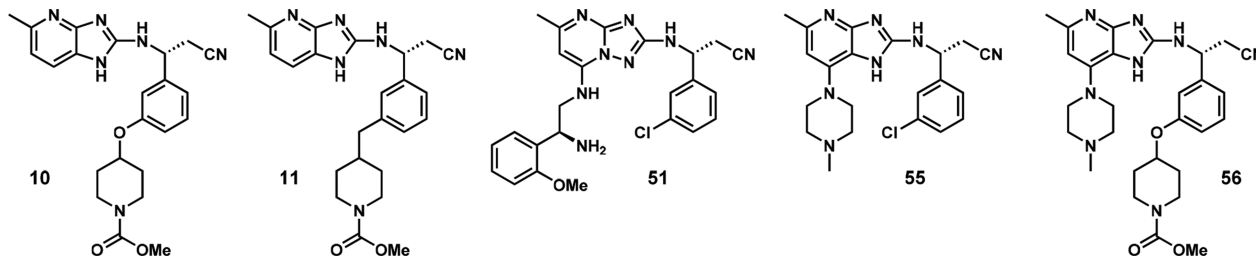
Analogs featuring the benzylic cyanomethyl substituent were prepared starting from 3-bromobenzaldehyde (**60**, **Scheme 2**), which was condensed with Ellman's (*R*)-*tert*-butanesulfonamide³⁰ to give **61**. Addition of the lithium anion of acetonitrile to imine **61** provided **62** as a single diastereomer following silica flash chromatography. Removal of the chiral auxiliary under acidic conditions and Boc protection of the resulting amine gave **63**, which could be further converted to the corresponding phenol (**64**) using Buchwald's conditions.³¹ Chan-Lam-Evans reaction of this phenol with (4-(methoxycarbonyl)phenyl)boronic acid gave the diphenyl ether **65** in reasonable yield, while nucleophilic displacement of the mesylate group from *N*-Cbz-4-mesyloxypiperidine yielded **67** (**Scheme 3**). Both intermediates were subjected to Boc-deprotection³² and subsequently converted to the triazolopyrimidinone as described previously for **7**. In the case of **69**, Cbz deprotection was followed by acylation with methyl chloroformate to give **9**.

Analogs featuring the azabenzimidazole core were derived from THP-protected 2-chloro-4-azabenzimidazole (**72**) which was prepared according to published precedent (**Scheme 4**).³³

Phenol **64** once again provided the starting point for ether-linked derivatives featuring the 4-azabenzimidazole core (**Scheme 5**). S_N2 displacement of the mesylate from methyl 4-mesyloxypiperidine-1-carboxylate gave **73**, which after Boc deprotection underwent Buchwald-Hartwig coupling³⁴ with 2-chloro-4-azabenzimidazole (**72**). THP deprotection (HCl, MeOH) of coupling product **74** provided **10**. Ether linked pyrrolidines **16** and **17** were prepared in a similar manner starting from (*S*)- or (*R*)-methyl-3-mesyloxypyrrolidine-1-carboxylate, respectively.

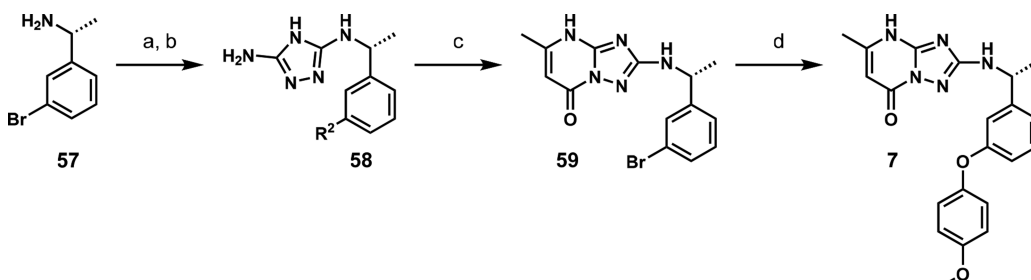
Azabenzimidazole derivatives **11**, **15**, **18**, and **19** were prepared starting from α -cyanomethylbenzylamine **63** (**Scheme 6**). Suzuki-Miyaura coupling with potassium vinyltrifluoroborate³⁵ provided styrene **77**, which was subjected to oxidative cleavage of the alkene followed by reduction of the resulting aldehyde to provide alcohol **79**. The Appel reaction³⁶ subsequently provided bromide **80**.

Alkylation of bromide **80** with piperazinone A (**Scheme 7**) provided **81**. Hydrogenolysis of the Cbz group was followed by acylation with methyl chloroformate; subsequent removal of the Boc group provided the primary amine which was subjected directly to Buchwald-Hartwig coupling with 2-chloro-4-azabenzimidazole **72**. Facile removal of the THP group under

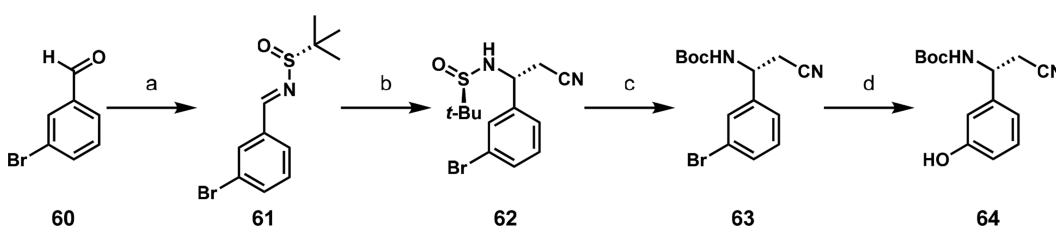
Table 8. *In Vitro* Characterization of Compounds 10, 11, 51, 55, and 56^a

	10	11	51	55	56
<i>E. coli</i> PPAT IC ₅₀ (nM)	11	9.3	3.9	35	9.1
<i>E. coli</i> PPAT SPR K _D (nM)	1.9	0.075	0.83	11	11
<i>E. coli</i> ΔtolC MIC (μg/mL)	0.25	<0.125	0.25	2	4
<i>E. coli</i> ΔacrB MIC (μg/mL)	32	16	1	8	64
<i>E. coli</i> imp4213 MIC (μg/mL)	8	2	1	8	64
<i>E. coli</i> WT MIC (μg/mL)	>128	128	32	64	>128
<i>E. coli</i> ΔtolC (coaSY)	>128	128	128	128	>128
<i>P. aeruginosa</i> WT MIC (μg/mL)	>128	>128	>128	>128	>128
<i>P. aeruginosa</i> OM* MIC (μg/mL)	128	NT	32	128	>128
<i>P. aeruginosa</i> ΔmexAB MIC (μg/mL)	128	32	16	>128	>128
MW	435	433	477	410	533
logD _{7.4}	3.0	2.8	3.1	2.6	NT
solubility (PBS, μg/mL)	264	158	74	>547	NT
microsomal stability (ER, r/h)	0.33/0.44	0.78/0.77	0.93/0.89	0.95/<0.3	0.69/0.56
Caco-2 P _{app} A→B (10 ⁻⁶ cm/s) (efflux ratio, B→A/A→B)	1.0 (48)	2.3 (18)	0.7 (82)	0.68 (72)	NT

^aNT = not tested. *P. aeruginosa* OM*: *P. aeruginosa* ATCC 35151, Z61 strain, a strain super susceptible to most antibiotics. Details of all strains are listed in Table 9.

Scheme 1. Synthesis of Triazolopyrimidinone 7^a

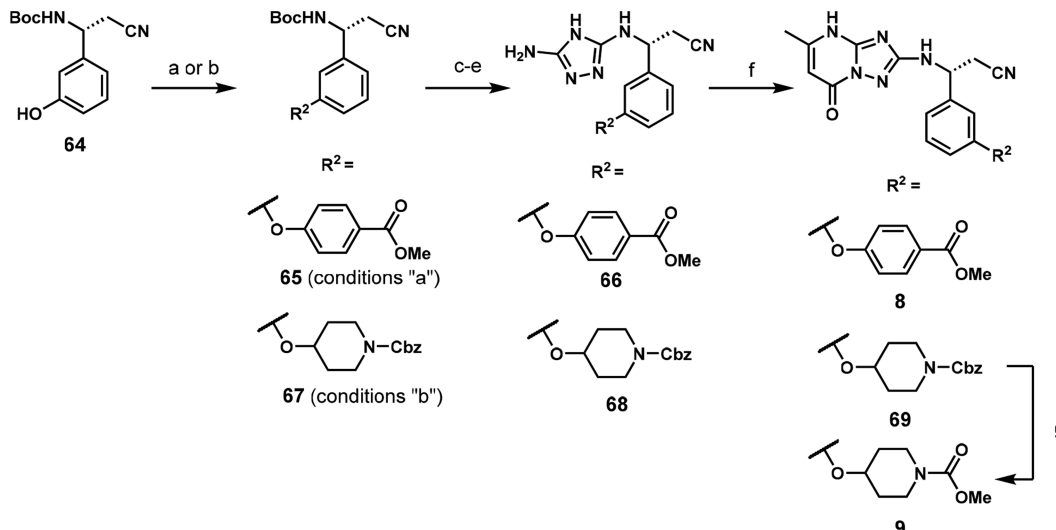
^a(a) diphenyl cyanocarbonimidate, 2-PrOH, 60 °C, 45 min. (b) hydrazine hydrate, MeOH, 50 °C, 4 h. (c) ethyl acetoacetate, AcOH, 165 °C, MW, 30 min, 86% (3 steps). (d) 4-methoxyphenol, Cs₂CO₃, CuCl, 2,2,6,6-tetramethyl-3,5-heptanedione, NMP, 120 °C, overnight, 14%.

Scheme 2. Synthesis of 3-Amino-3-phenylpropanenitrile Intermediates^a

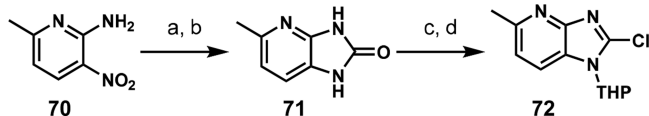
^a(a) (R)-*tert*-butanesulfonamide, CuSO₄, MgSO₄, PPTS, CHCl₃, reflux, 16 h, 97%. (b) LiN(*i*-Pr)₂, MeCN, THF, -78 °C, 30 min then 61, THF, -78 °C, 2.5 h, 38%. (c) 1. HCl (4 M in dioxane), MeOH-Et₂O (1:1), rt, 1 h; 2. *i*-Pr₂NEt, (Boc)₂O, 0 °C → rt, 2.5 h, 85%. (d) *t*-BuXPhos, Pd₂(dba)₃, KOH, 1,4-dioxane, water, 60 °C, 2 h, 29%.

acidic conditions gave 15. A similar route was employed to prepare 11, 18, and 19. Suzuki-Miyaura coupling with boronate pinacol esters B or C delivered 83 and 85 respectively in high yield. Hydrogenolysis of the Cbz group with concomitant reduction of the olefin was followed by acylation with methyl

chloroformate. As before, Boc deprotection and Buchwald-Hartwig coupling with 72 provided the final compounds smoothly following THP deprotection. In the case of pyrrolidine 87, the diastereomers were separated by chiral HPLC to give 18 and 19.³⁷

Scheme 3. Synthesis of Triazolopyrimidinones 8 and 9^a

^a(a) (4-(methoxycarbonyl)phenyl)boronic acid, Cu(OAc)₂, Et₃N, CH₂Cl₂, 4 Å MS, rt, overnight, 51%. (b) benzyl 4-((methanesulfonyl)oxy)piperidine-1-carboxylate, Cs₂CO₃, DMF, 60 °C, 5.5 h, 59%. (c) 1,1,1,3,3-hexafluoroisopropanol, 150 °C, MW, 15 min. (d) diphenyl cyanocarbonimidate, 2-PrOH, rt, overnight. (e) hydrazine hydrate, 2-PrOH, rt, 3–5 h. (f) ethyl acetoacetate, AcOH, 4 Å MS, 100 °C, 1–2 h, 8% (8) or 62% (69). (g) 1. H₂, Pd/C, MeOH, THF; 2. methyl chloroformate, iPr₂NEt, CH₂Cl₂, rt, 24%.

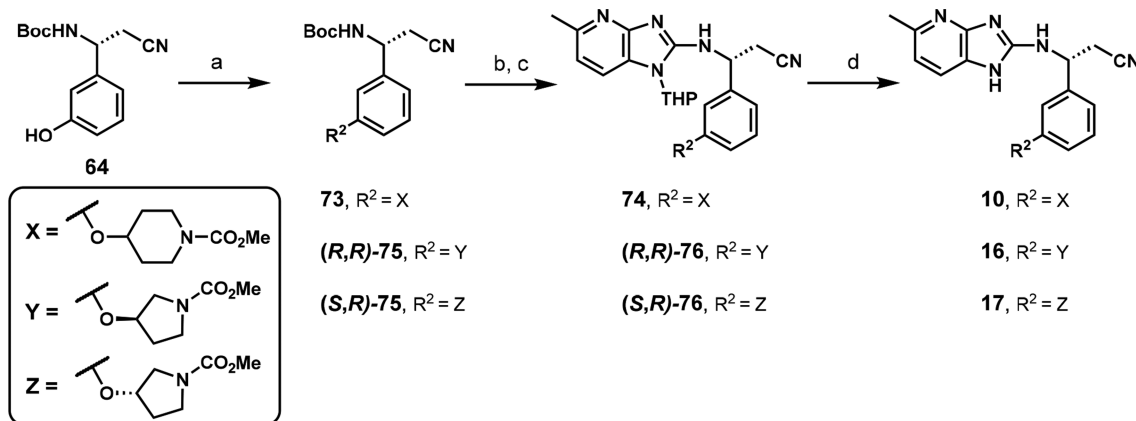
Scheme 4. Synthesis of 2-Chloro-4-azabenzimidazole 72^a

^a(a) Pd/C, H₂, EtOH-EtOAc, overnight. (b) CDI, THF, rt, 98% (2 steps). (c) POCl₃, 95 °C, overnight. (d) 3,4-dihydro-2H-pyran, p-TsOH-H₂O, THF, reflux, 2 h, 32% (2 steps).

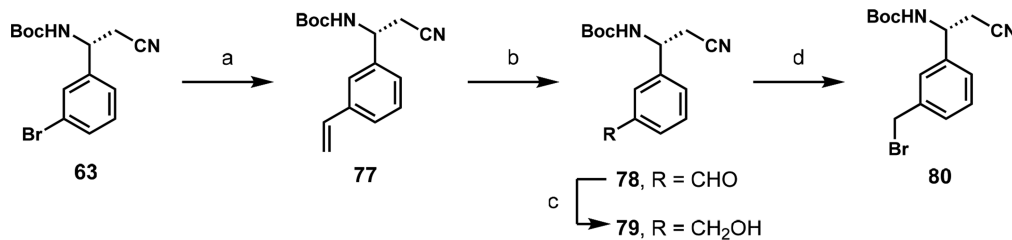
Synthesis of 12–14 is described in Scheme 8. Thioether 88 was prepared by direct coupling of methyl 4-(acetylthio)piperidine-1-carboxylate with bromide 63 using a modification of literature conditions.³⁸ Compound 88 was converted to 12 by a three-step sequence involving Boc deprotection,

Buchwald-Hartwig coupling with 72, and THP deprotection. Alternatively, oxidation of 88 with Oxone provided the sulfone 90 in good yield. Subjection of 90 to the same three-step sequence gave 13. Sulfonamide 92 was prepared directly and in good yield from the aryl bromide using a recently published³⁹ three-step/one-pot protocol involving generation of the sulfinate salt, followed by treatment with NBS to give the sulfonyl bromide which reacted rapidly with N-Cbz piperazine to give 93. After Boc deprotection and Buchwald-Hartwig coupling the Cbz group was removed, and the resulting amine converted to the desired methyl carbamate 14.

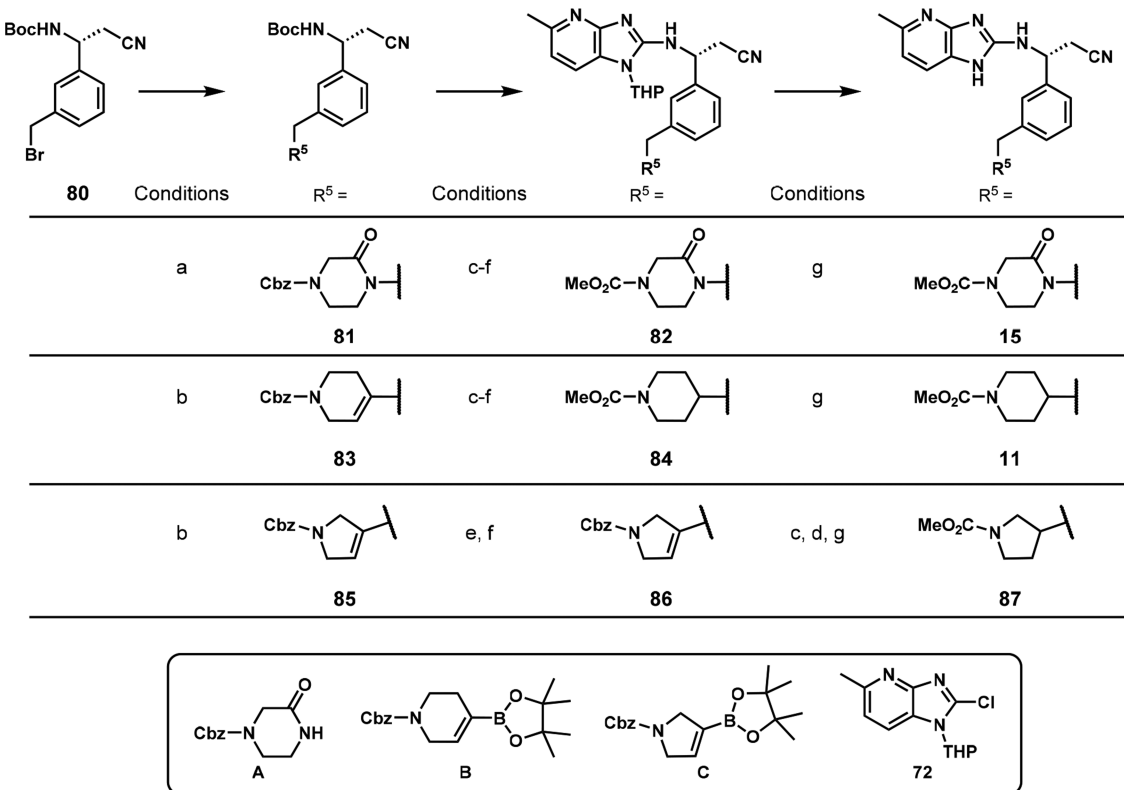
Compounds 20–27 were synthesized as described in Schemes 9 and 10. SmI₂-mediated addition of benzyl bromide 80 to N-Cbz-4-oxopiperidine provided the tertiary alcohol 94, which after Boc deprotection underwent palladium-catalyzed

Scheme 5. Synthesis of 4-Azabenzimidazole Analogs 10, 16, and 17^a

^a(a) 73: methyl 4-((methylsulfonyl)oxy)piperidine-1-carboxylate, Cs₂CO₃, DMF, 60–80 °C, 65%; (R,R)-75: (S)-methyl-3-mesyloxypyrrolidine-1-carboxylate, Cs₂CO₃, MeCN, 120 °C, MW, 1 h, 63%; (S,R)-75: (R)-methyl-3-mesyloxypyrrolidine-1-carboxylate, Cs₂CO₃, MeCN, 120 °C, MW, 1 h, 37%. (b) 74: HCl (4 M in dioxane), Et₂O-MeOH (1:1), rt; 76: 1,1,1,3,3-hexafluoroisopropanol, 150 °C, MW, 15 min. (c) 72, Pd₂(dba)₃, BINAP, NaOtBu, toluene, 85 °C, overnight, 77% for 74, 64% for (R,R)-76, 54% for (S,R)-76. (d) HCl (4 M in dioxane), MeOH-Et₂O (1:1), rt, 97% for 10, 27% for 16, 10% for 17.

Scheme 6. Synthesis of 3-Amino-3-phenylpropanenitrile Intermediate 80^a

^a(a) potassium vinyltrifluoroborate, Pd(OAc)₂, PPh₃, Cs₂CO₃, THF–H₂O (9:1), 85 °C, 18 h, 68%. (b) ozone, CH₂Cl₂, –78 °C, then PS-PPh₃, –78 °C → rt. (c) NaBH₄, MeOH, 0 °C, 30 min, 61% (2 steps). (d) CBr₄, PPh₃, CH₂Cl₂, 0 °C, 1.5 h, 76%.

Scheme 7. Synthesis of 4-Azabenzimidazoles 11, 15, 18, and 19^a

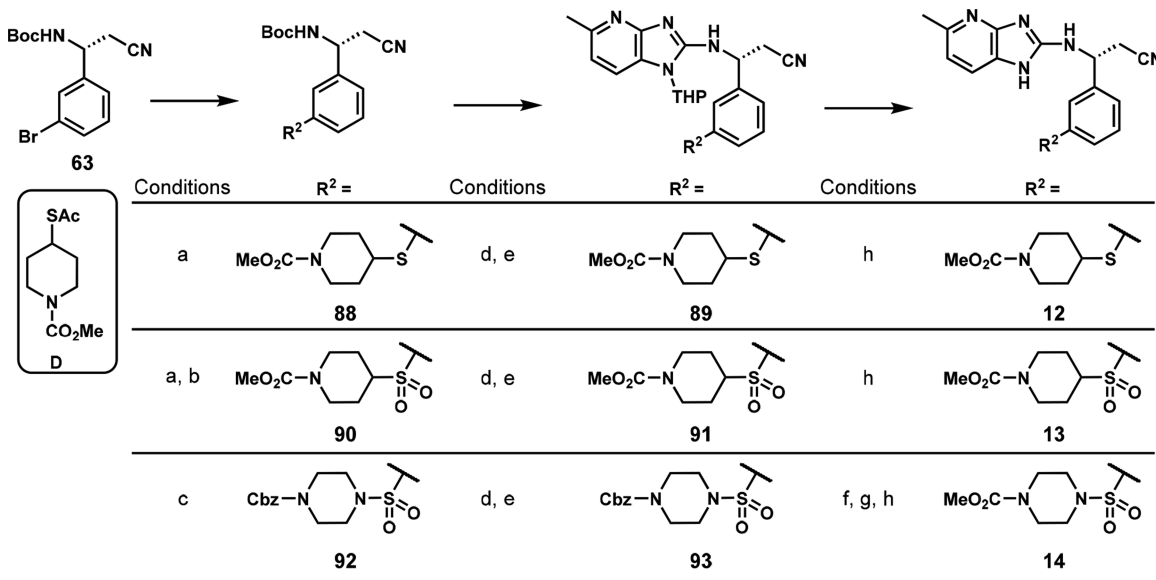
^a(a) A, NaH, DMF, 0 °C, 30 min then 80, rt, 1.5 h, 71%. (b) B or C, Pd(PPh₃)₄, Cs₂CO₃, THF–H₂O (3:1), 120 °C, MW, 30 min; quant. for 83, 88% for 85. (c) H₂, Pd/C, EtOAc or EtOH, rt, 4 h – overnight. (d) methyl chloroformate, Et₃N, CH₂Cl₂ or THF, 0 °C → rt. (e) 1,1,1,3,3,3-hexafluoroisopropanol, 150 °C, MW, 15–20 min. (f) 72, Pd₂(dba)₃, BINAP, NaOtBu, toluene, 85 °C, overnight; 48% for 82 (4 steps from 81), 71% for 86 (2 steps from 85). (g) HCl, MeOH/dioxane/Et₂O; 9% for 15, 25% for 11 (5 steps from 83), 86% for 87 (3 steps from 86).

arylation with 72, followed by THP removal to furnish 20. Alternatively, benzyl bromide 80 could be cleanly alkylated with the enolate derived from dimethylpiperidine-1,4-dicarboxylate. Boc deprotection and Buchwald–Hartwig coupling with 72 provided the key intermediate 97. Reduction with LiBH₄ gave primary alcohol 98, which after THP deprotection provided 21. Alternatively, oxidation of 98 under Swern conditions⁴⁰ provided aldehyde 99 (Scheme 10). Subsequent Pinnick oxidation⁴¹ gave the corresponding carboxylic acid 22 after THP deprotection. From the aldehyde, reductive amination followed by THP deprotection yielded amine 27, while condensation with O-methylhydroxylamine provided the oxime 23 after deprotection. Aldehyde 99 was also subjected to Horner–Wadsworth–Emmons olefination⁴² with phosphonate E which resulted in concomitant removal of the THP group. Hydrogenation then provided 26. In a similar manner,

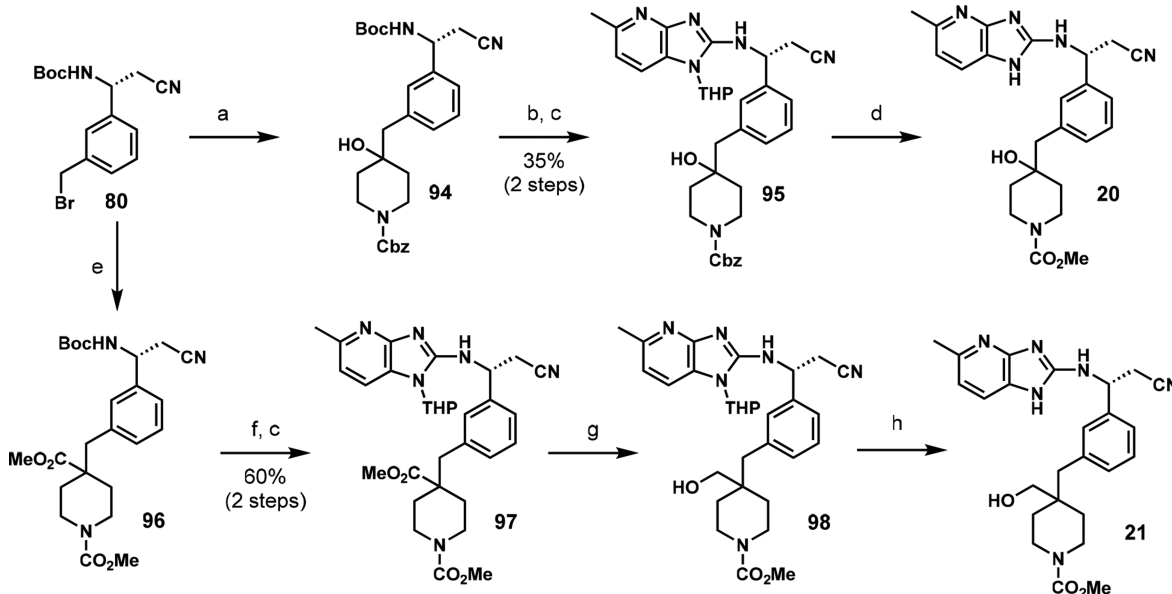
the HWE reaction with phosphonate F gave α,β -unsaturated ester 100. Hydrogenation and THP cleavage provided 101 which was subsequently reduced to alcohol 24 or hydrolyzed to acid 25.

To access 7-amino triazolopyrimidines 29–39 and 42, the appropriate triazolopyrimidinone was treated with neat POCl₃ at reflux to give the 7-chloro-triazolopyrimidine intermediates 102 and 103 in high yield (Scheme 11). These intermediates were then treated with a stoichiometric excess of myriad commercially available amines in ethanol to provide the desired final products. While many nucleophilic aromatic substitutions (S_NAr) were found to progress nicely at room temperature, reactions that employed poorly nucleophilic amines required heating.

In instances where the amine S_NAr partner was not commercially available, such as the diamines found in Table

Scheme 8. Synthesis of 4-Azabenzimidazoles 12–14^a

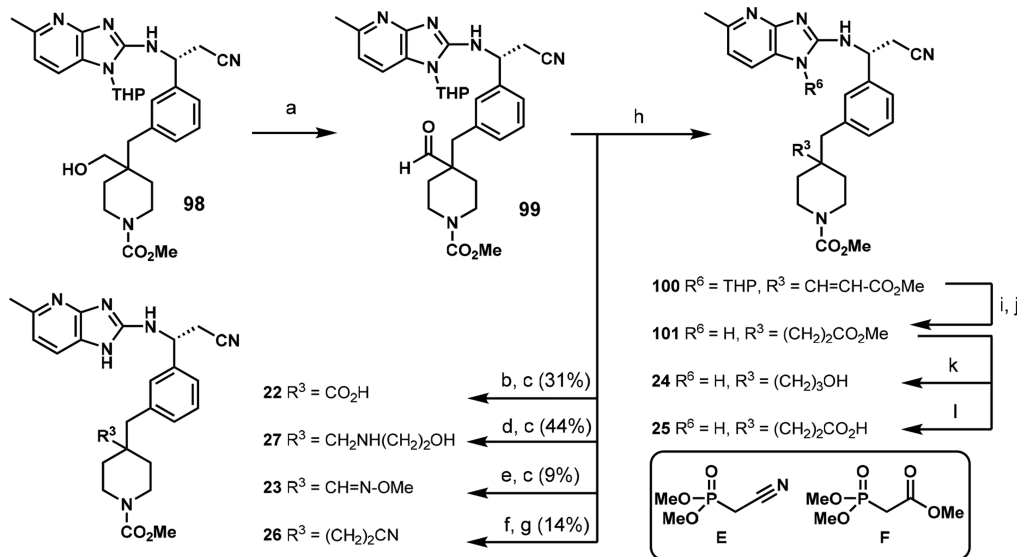
^a(a) D, $\text{Pd}_2(\text{dba})_3$, DPPF, NaOtBu, toluene, 110 °C, 4 h, 78%. (b) Oxone, MeOH, rt, 5.5 h, 81%. (c) $\text{Pd}(\text{OAc})_2$, PPh_3 , 1,10-phenanthroline, Bu_4NBr , HCO_2Na , $\text{K}_2\text{S}_2\text{O}_5$, DMSO, 70 °C, 4 h then N-Cbz-piperazine, NBS, THF, 0 °C → rt, 1 h, 55%. (d) 1,1,1,3,3-hexafluoroisopropanol, 150 °C, MW, 15 min. (e) 72, $\text{Pd}_2(\text{dba})_3$, BINAP, NaOtBu, toluene, 85 °C, overnight; 55% for 89, 38% for 91, 31% for 93 (2 steps). (f) H_2 , Pd/C, EtOH/EtOAc, rt, 4 h. (g) Methyl chloroformate, $i\text{Pr}_2\text{NEt}$, CH_2Cl_2 , rt. (h) HCl, dioxane, MeOH, rt; 41% for 12, 32% for 13, 30% for 14 (3 steps from 93).

Scheme 9. Synthesis of 4-Azabenzimidazoles 20 and 21^a

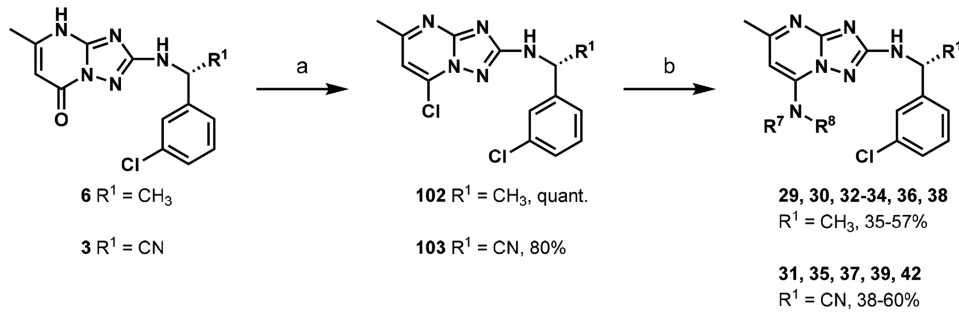
^a(a) N-Cbz-4-oxopiperidine, SmI_2 , THF, rt, 1 h, 79%. (b) 1,1,1,3,3-hexafluoroisopropanol, 150 °C, MW, 15 min. (c) 72, $\text{Pd}_2(\text{dba})_3$, BINAP, NaOtBu, toluene, 85 °C, 15 h (95) or 160 °C, 1 h (97). (d) 1. H_2 , Pd/C, EtOH, EtOAc, 4 h; 2. methyl chloroformate, $i\text{Pr}_2\text{NEt}$, CH_2Cl_2 ; 3. 4 M HCl in dioxane, MeOH, rt, 15 min, 35%. (e) dimethylpiperidine-1,4-dicarboxylate, NaHMDS, THF, −78 °C, quant. (f) 4 M HCl in dioxane, MeOH. (g) LiBH₄, THF-MeOH (5:1), 60 °C, overnight, 81%. (h) 4 M HCl in dioxane, MeOH, Et_2O , rt, 30 min, 8%.

⁷, the desired amine was prepared by different routes depending upon the building blocks that were commercially available at the time of synthesis (Schemes 12 and 13). Straightforward preparation of the appropriate N-Boc-protected 1,2-amino alcohol precursors in Scheme 12 was achieved either by direct reduction of N-Boc amino acids 104a–d with cold Red-Al⁴³ or Boc protection of 1,2-amino alcohols 105e–k. From here, a three-step sequence comprising mesylation of the

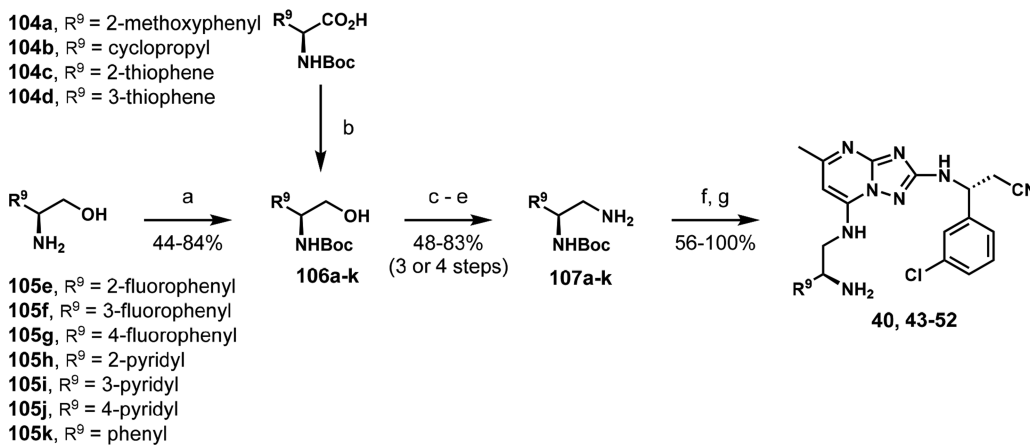
primary alcohol, S_N2 displacement of the resulting mesylate with sodium azide, and alkyl azide reduction provided the primary amine $S_N\text{Ar}$ partners 107a–k. On a small scale, it was convenient to carry out the azide reduction with polymer-bound triphenylphosphine in wet THF; however, palladium-catalyzed hydrogenolysis was preferable on a larger scale. Union of the appropriate N-Boc-protected diamine with 7-chlorotriazolopyrimidine intermediate 103 in the presence of a

Scheme 10. Synthesis of 4-Azabenzimidazoles 22–27^a

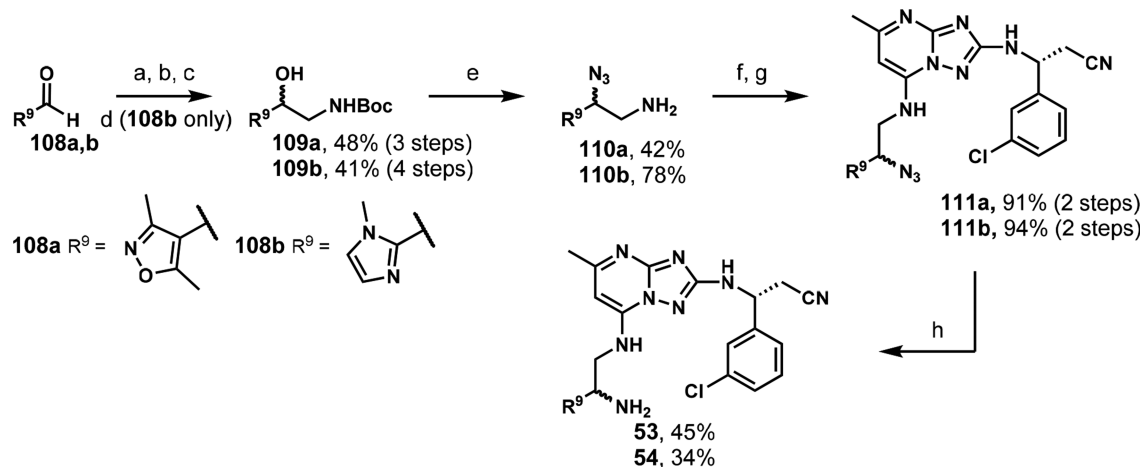
^a(a) (COCl)₂, DMSO, Et₃N, CH₂Cl₂, -78 °C → rt, 30 min, quant. (b) NaO₂Cl, 2-methyl-2-butene, NaH₂PO₄, THF-tBuOH-water (3:5:1), rt, 45 min. (c) 4 M HCl in dioxane, MeOH, rt, 15 min – 2 h. (d) 2-aminoethanol, acetic acid, MeOH, 60 °C, 1 h then NaBH(OAc)₃, 60 °C, 16 h. (e) O-methylhydroxylamine hydrochloride, Na₂CO₃, EtOH, rt, 1 h. (f) E, NaH, THF, 0 °C, 15 min then 99, 0 °C → rt, 16 h. (g) H₂, Pd/C, MeOH, rt. (h) F, NaH, THF, 0 °C, 15 min then 99, 0 °C → rt, 16 h, 76%. (i) H₂, Pd/C, MeOH, rt. (j) 4 M HCl in dioxane, MeOH, rt, 15 min. (k) LiBH₄, THF-MeOH (2:1), 60 °C, 2 h, 23%. (l) 1 M NaOH(aq), THF-MeOH (2:1), rt, 1 h, 54%.

Scheme 11. Synthesis of Triazolopyrimidines 29–39 and 42^a

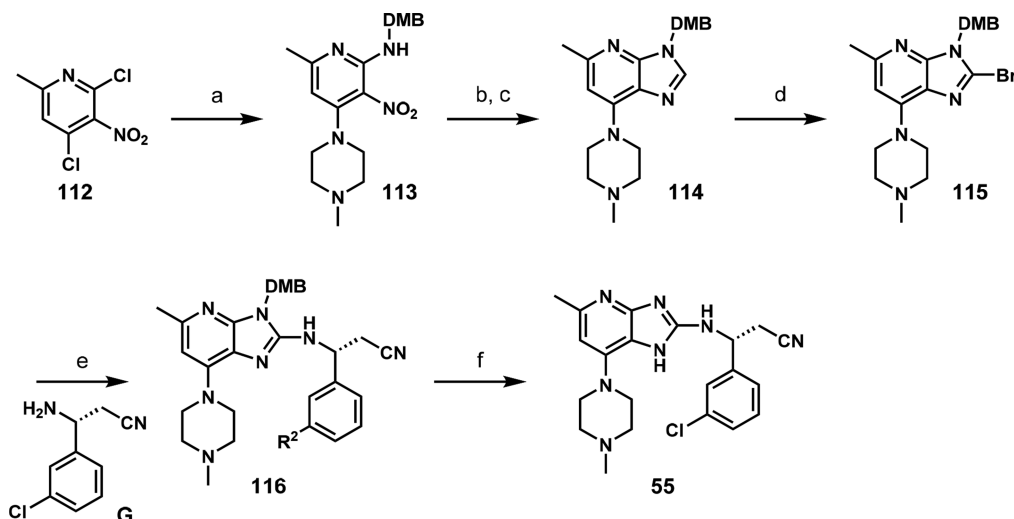
^a(a) POCl₃, reflux. (b) R⁷R⁸NH, EtOH, rt or 70 °C.

Scheme 12. Synthesis of Triazolopyrimidines 40, 41, and 43–52^a

^a(a) (Boc)₂O, Et₃N, CH₂Cl₂, 0 °C → rt, 1 h. (b) Red-Al (65 wt % in toluene), THF, 0 °C, 2 h. (c) MsCl, Et₃N, CH₂Cl₂, 0 °C. (d) NaN₃, DMF, 60 °C. (e) Pd/C, H₂, EtOH, rt. (f) 103, Et₃N, EtOH, 70 °C. (g) TFA, CH₂Cl₂, rt.

Scheme 13. Synthesis of Triazolopyrimidines 54 and 55^a

^a(a) TMSCN, ZnI₂, DCM, rt, 3 h. (b) LiAlH₄, THF, 0 °C → rt, 2 h. (c) (Boc)₂O, Et₃N, CH₂Cl₂ 0 °C → rt, 2 h. (d) NaOH, MeOH, water, rt, 16 h. (e) DPPA, DBU, toluene, 0 °C, 1 h then rt, 16 h. (f) TFA, CH₂Cl₂, rt, 1 h. (g) 103, Et₃N, EtOH, 70 °C, 16 h. (h) H₂, Pd/C, EtOAc, rt, 16 h.

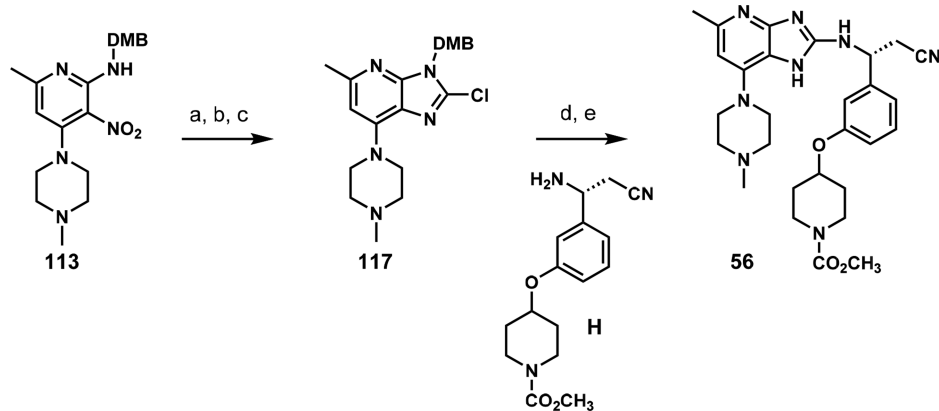
Scheme 14. Synthesis of 4-Azabenzimidazole 55^a

^a(a) N-methylpiperazine, Et₃N, EtOH, rt, 3.5 h then 2,4-dimethoxybenzylamine, reflux, overnight, 52%. (b) Zn dust, saturated aqueous NH₄Cl, THF, MeOH, 0 °C → rt. (c) (MeO)₃CH, p-TsOH·H₂O, 100 °C, 30 min, 62% (2 steps). (d) n-BuLi, THF, -40 °C, 30 min then CBr₄, -40 → 0 °C, 2 h, 60%. (e) Pd₂(dba)₃, BINAP, NaOtBu, toluene, 85 °C, 4.5 h. (f) TFA-toluene (1:1), rt, 3 h, 18% (2 steps).

tertiary amine base in hot ethanol, followed by Boc deprotection with TFA, provided the desired analogs. Compound 41 was prepared using an identical route starting from the corresponding *N*-Boc-*d*-phenylglycinol (see the Supporting Information for details). Alternatively, some heterocycle-derived 1,2-diamines were accessed from the parent aldehyde as shown in Scheme 13. Here, ZnI₂-mediated cyanohydrin formation, nitrile reduction with LiAlH₄, and Boc protection of the resultant amino alcohol, which were regioisomeric with those in Scheme 12, allowed us to employ the excellent method introduced by the process chemistry department at Merck to directly convert the benzylic alcohol to the azide.⁴⁵ The desired primary amines were unveiled from the orthogonally protected diamines by acidic removal of the Boc group.⁴⁶ As before, S_NAr reactions with 7-chloro-triazolopyrimidine intermediate 103 proceeded well, and the final compounds could be obtained after palladium-catalyzed hydrogenolysis of the secondary alkyl azide. These compounds

were frequently submitted as diastereomeric mixtures in the first pass, after which the most promising mixtures were subjected to separation by chiral chromatography and data were obtained for each pure diastereomer.

The 7-amino imidazolopyridines required a new route as limited studies directed at late-stage C7 functionalization of the parent core failed to provide a robust method. We ultimately settled on the synthesis shown in Scheme 14. While this route offered limited opportunity for systematic variation of the C7 substituent, it was robust and allowed us to access sufficient material to explore the beneficial effect (*vide supra*) of the *N*-methylpiperazine substituent in the context of the more potent imidazolopyridine core. Beginning with commercially available 2,4-dichloro-6-methyl-3-nitropyridine, a one-pot diamination was achieved by temperature-controlled, sequential addition of *N*-methylpiperazine and 2,4-dimethoxybenzylamine at the 4- and 2-positions, respectively, in the presence of excess Et₃N to provide compound 113. Reduction of the nitro group with Zn-

Scheme 15. Synthesis of 4-Azabenzimidazole 56^a

^a(a) Zn dust, saturated aqueous NH₄Cl, THF, MeOH, 0 °C → rt. (b) CDI, THF, rt, overnight. (c) POCl₃, i-Pr₂NEt, 110 °C, overnight, 69% (3 steps). (d) Pd₂(dba)₃, BINAP, NaOtBu, toluene, 110 °C, overnight. (e) TFA, toluene, rt, 3 h, 10% (2 steps).

NH₄Cl was followed by imidazole formation in hot trimethylorthoformate in the presence of *p*-TsOH. Several of the more traditional methods for bromination of imidazolopyridine 114 at the 2-position were complicated by bromination of the DMB group, but trapping of the lithiated species with CBr₄ returned the desired 2-bromo imidazolopyridine 115 in good yield. Buchwald-Hartwig coupling with the appropriate benzylamine and TFA-mediated deprotection of the DMB group completed the synthesis of imidazolopyridine 55. Ether-linked piperidine analog 56 was accessed using a similar route in which 2-chloro-4-azabenzimidazole 117 underwent Buchwald coupling with amine H, followed by removal of the DMB under acidic conditions (Scheme 15).

CONCLUSIONS

The discovery of new antibacterial agents that inhibit noncanonical targets is a critical goal in the ongoing battle against antibiotic resistance. Historically, the translation of hits discovered from target-based HTS efforts into leads with whole-cell activity against Gram-negative bacteria has been extremely challenging. Against PPAT from Gram-negative bacteria, we chose to pursue an FBLD approach which resulted in the identification of several unique scaffolds that bound in the phosphopantetheine pocket of the PPAT active site.¹⁹ Aided by a robust crystallographic soaking system, several fragments with micromolar potency against PPAT were selected and optimized to give leads such as 3 and 4, which exhibited nanomolar biochemical IC₅₀ values and modest cellular activity against *E. coli* Δ*tolC*.

Achieving measurable growth inhibition against WT Gram-negative bacteria proved a major hurdle for the program, which to some degree was expected. Taking advantage of a wealth of fragment-bound X-ray cocrystal structures we successfully designed and prepared analogs with improved on-target potency, such as piperidine carbamate 9. The discovery that compounds featuring an azabenzimidazole core enjoyed improved Gram-negative permeability ultimately paved the way for the identification of the first compounds with whole-cell activity against WT *E. coli* (e.g., 19). Unfortunately, issues associated with bacterial efflux limited the further progression of this series.

A key breakthrough in this campaign was the observation that the incorporation of a weakly basic amine afforded compounds with robust Gram-negative permeability as well as

improved physicochemical properties (e.g., 37). Combining this structural feature with moieties capable of engaging in π-stacking interactions with Y98 yielded compounds with subnanomolar binding affinity and MICs against WT *E. coli* as low as 32 μg/mL (e.g., 51). Incorporation of a weakly basic piperazine into compounds featuring the azabenzimidazole core yielded 55, a compact and efficient molecule that inhibited the growth of WT *E. coli* and exhibited improved permeability and reduced efflux compared to progenitor compounds in the series.

The progression from fragment hit to lead compound was marked by an increase in biochemical potency of 4–5 orders of magnitude. Equally important to our optimization efforts were several observations on Gram-negative permeability enabled by a combination of MS-based metabolomics data and traditional MIC measurement against WT and mutant *E. coli* strains. Compounds such as 51 and 55 represent the first known bacterial PPAT inhibitors with cellular activity against WT Gram-negative bacteria. Unfortunately, sufficient potency against representative Gram-negative species could not be obtained to warrant further development of this series. Although none of the series disclosed in this or the accompanying manuscript yielded a clinical candidate, it is our hope that these studies will help pave the way toward the discovery of new Gram-negative antibacterial agents with novel modes of action.

EXPERIMENTAL SECTION

General. All key compounds (3, 4, 6–19, 20–27, 29–56) possess a purity of at least 95% as assessed by analytical reversed phase HPLC (see the Supporting Information for details). IC₅₀ values obtained from biochemical and metabolite assays are reported as the average of two or more replicates. For MIC data, the most frequently occurring value from three or more replicates is reported. In cases where two values occurred with identical frequency, the higher of the two values is reported. MIC data for compounds 6, 25, 36, and 53 are from a single replicate. MIC data for compound 11 against *E. coli* Δ*acrB* represents a single replicate. See Table 9 for a description of all bacterial strains used in this study. SPR K_D for compounds 10, 12, 17, 23, 25, 30, 35, 37, 42, and 51 are an average of two or more replicates. For all other compounds SPR K_D values are from a single replicate.

Biochemical Assay. All enzymes were expressed with C-terminal His tags and purified in-house from *E. coli*. All biochemical reactions were carried out in a buffer consisting of 50 mM Tris pH 7.5, 50 mM KCl, 5 mM DTT, 1 mM MgCl₂, 0.01% (w/v) BSA, 0.01% (w/v) P20.

Table 9. Strains and Plasmids Used in This Study^a

code	referred to as	description	source or ref
<i>P. aeruginosa</i>			
PAO1	<i>P. aeruginosa</i> WT	K767; PAO1, prototroph	47
ATCC 35151	<i>P. aeruginosa</i> OM	Z61, mutant 61 isolated by mutagenesis of ATCC 12055 and selection for antibiotic super susceptibility, prototroph	48
K1119	<i>P. aeruginosa</i> Δ mexAB	K767 Δ mexAB-oprM	49
<i>E. coli</i>			
BW25113	<i>E. coli</i> WT	BW25113	50
JW5503-1	<i>E. coli</i> Δ tolC	BW25113 Δ tolC	50
JW0451-2	<i>E. coli</i> Δ acrB	BW25113 Δ acrB	50
RFM795	<i>E. coli</i> imp4213	in frame deletion of 23 amino acids (D330 to D352) in lptD gene in <i>E. coli</i> MC4100	51
JWK0002	<i>E. coli</i> Δ tolC, coaSY	<i>E. coli</i> Δ tolC::FRT Δ coaD::aph (Km ^R), + pNOV016 (pBRori lacI P _{lac} :: coaSY _{hs} aacC1 (Gm ^R))	this study
Plasmids			
pNOV016		IPTG inducible coaSY _{hs} expression vector, (pBRori, lacI, P _{lac} :: coaSY _{hs} , aacC1 (Gm ^R))	this study

^aGm^R, gentamicin resistance marker; Km^R, kanamycin resistance marker.

4'-Phosphopantetheine, the substrate for PPAT/CoaD, was synthesized biosynthetically by incubating 12 μ M *E. coli* PanK/CoaA enzyme with 10 mM ATP (Sigma) and 5 mM pantethine (Sigma) overnight at rt. This reaction produced two molecules of 4'-phosphopantetheine per molecule of pantethine and in the process consumed 2 molecules of ATP. The next morning, the ATP in the reaction was quantified to ensure the reaction had run to completion.

PPAT/CoaD activity was measured by coupling the production of pyrophosphate from the PPAT/CoaD reaction to the production of inorganic phosphate by pyrophosphatase. Inorganic phosphate was then quantified using the BIOMOL Green reagent and measuring the absorbance at 620 nm. Reactions were set up by incubating 24 nM CoaD (PPAT), 200 μ M ATP (2X measured K_m), and the compound together in assay buffer for 5 min and initiated by the addition of 20 μ M 4'-phosphopantetheine and 78 nM pyrophosphatase. Reactions were allowed to proceed for 30 min at rt before being stopped through addition of a volume of BIOMOL Green reagent equal to the reaction volume. Compounds were delivered in sufficient concentrations to result in a final concentration of DMSO in each reaction of less than 5%.

Conditions for the biochemical assay with *P. aeruginosa* PPAT were identical with the exception of enzyme concentration, which was 17.4 nM.

SPR. Using a Biacore T200, Avi-tagged CoaD was immobilized to a Biacore SA chip, and any unbound streptavidin was blocked with biocytin (Sigma-Aldrich). Compounds were tested individually at varying concentrations in running buffer (50 mM HEPES pH 7.0, 150 mM KCl, 1 mM TCEP, 0.05% Tween 20, 2% DMSO) at 20 °C. Sensograms were run in order from low to high concentration using a flow rate of 80 μ L/min. All sensor chips were monitored for loss of activity with the injection of a control compound that retains >75% of the activity over the course of the run. Analysis of the binding curves and determination of the kinetic parameters were performed using evaluation software (Version 2.0, Biacore).

Susceptibility Testing. Susceptibility testing was performed using a broth microdilution assay following the recommended methodology of the Clinical and Laboratories Institute (CLSI) (REF: CLSI M7-A9). In brief, fresh bacterial overnight colony growth was resuspended in sterile saline, adjusted to a 0.5 McFarland turbidity standard, and then diluted 1:200 into cation-adjusted Mueller-Hinton Broth II (CAMHB; Becton Dickinson, Franklin Lakes, NJ) to yield a final target inoculum

of 5×10^5 colony-forming units (CFU)/mL. Twofold serial dilutions of compounds were prepared in 100% DMSO at 100-fold the highest final assay concentration; the resulting dilution series of compounds were diluted 1:10 with sterile water. Assay microtiter plates, which contained 10 μ L of 10-fold final concentration of compound per well, were inoculated with a volume of 90 μ L of bacterial inoculum, sealed in a plastic bag to prevent moisture loss, and incubated for 20 h at 35 °C in ambient air. Following incubation, assay plates were monitored for bacterial growth with a SPECTRAmax380 microtiter plate reader (Molecular Devices, Sunnyvale, CA) at 600 nm, as well as by visual observation with a reading mirror. The minimal inhibitory concentration (MIC) is defined as the lowest concentration of antibiotic at which the visible growth of the organism is completely inhibited. Performance of the assay was monitored by testing gatifloxacin against laboratory quality control strains in accordance with guidelines of the CLSI (REF: CLSI M100-S22).

REF CLSI M7-A9. Clinical Laboratory Standards Institute (CLSI). Methods for dilution antimicrobial susceptibility tests for bacteria that grow aerobically: approved standard - Ninth edition. CLSI document M07-A9. Wayne, PA; 2012.

REF CLSI M100-S22. Clinical Laboratory Standards Institute (CLSI). Performance Standards for Antimicrobial Susceptibility Testing; Twenty-Second Informational Supplement. CLSI document M100-S22. Wayne, PA; 2012.

Chemistry. *Methyl (R)-4-(3-(2-Cyano-1-((5-methyl-1*H*-imidazo[4,5-*b*]pyridin-2-yl)amino)ethyl)phenoxy)piperidine-1-carboxylate (10).* 74 (1.1 g, 2.12 mmol) was dissolved in MeOH (50 mL) and Et₂O (50 mL). HCl (4 M in dioxane, 0.64 mL, 2.55 mmol) was added. The clear, pale yellow mixture was stirred at room temperature for 30 min. Triethylamine (0.44 mL, 3.18 mmol) was added. The mixture was concentrated to dryness under reduced pressure to give the crude product as a yellow solid. SiO₂ flash chromatography (0 → 10% MeOH/DCM) provided 500 mg of the desired product as a white solid. Repurification by SFC chromatography provided **10** (306 mg, 97%) as a white powder.

Compound **10** and other compounds featuring the 4-azabenzimidazole core were often observed by NMR to interconvert between two tautomeric forms (or possibly conformational isomers). As a result, ¹H NMR peaks for protons attached to, or near, the core heterocycle were often observed to "split" in DMSO-d₆. For compound **10** a single set of well-resolved ¹H NMR peaks was observed in methanol-d₄. A listing of ¹H NMR data is provided below in both solvents.

¹H NMR (400 MHz, DMSO-d₆) δ 11.41 (s, 0.5 H), 10.82 (s, 0.5H), 7.79 (d, J = 6.2 Hz, 0.5 H), 7.54 (d, J = 8.9 Hz, 0.5H), 7.36–7.22 (m, 2H), 7.12 (s, 1H), 7.05 (d, J = 7.5 Hz, 1H), 6.94–6.86 (m, 1H), 6.79 (d, J = 7.9 Hz, 0.5H), 6.69 (d, J = 7.7 Hz, 0.5H), 5.21 (q, J = 7.5 Hz, 1H), 4.55 (m, 1H), 3.74–3.62 (m, 2H), 3.59 (s, 3H), 3.26–3.18 (m, 2H), 3.18–3.09 (m, 2H), 2.40 (s, 1.5H), 2.38 (s, 1.5H), 1.97–1.86 (m, 2H), 1.52 (td, J = 12.9, 8.6, 3.9 Hz, 2H). ¹H NMR (500 MHz, methanol-d₄) δ 7.40 (d, J = 7.8 Hz, 1H), 7.29 (t, J = 8.0 Hz, 1H), 7.11 (t, J = 2.1 Hz, 1H), 7.08–7.05 (m, 1H), 6.91 (ddd, J = 8.3, 2.5, 0.8 Hz, 2H), 6.85 (d, J = 7.9 Hz, 1H), 5.27 (t, J = 6.7 Hz, 1H), 4.55 (m, 1H), 3.73–3.67 (m, 2H), 3.68 (s, 3H), 3.38–3.32 (m, 2H), 3.20–3.10 (m, 2H), 2.48 (s, 3H), 1.95–1.86 (m, 2H), 1.70–1.60 (m, 2H). [α]_D²⁰ + 67.8 (c 1.0, MeOH). HRMS (ESI): m/z 435.2150 [M + H]⁺.

*Methyl (R)-4-(3-(2-Cyano-1-((5-methyl-1*H*-imidazo[4,5-*b*]pyridin-2-yl)amino)ethyl)benzyl)piperidine-1-carboxylate (11).* Intermediate **84** (55 mg, 0.106 mmol) was dissolved in 1:1 MeOH-Et₂O (0.8 mL) and treated with 4 M HCl in dioxane (37 μ L, 0.149 mmol). After stirring at rt for 30 min triethylamine (21 μ L, 0.149 mmol) was added, and volatiles were evaporated under reduced pressure. Purification by preparative RP-HPLC provided **11** (11.7 mg, 25%) as a white powder.

¹H NMR (400 MHz, DMSO-d₆) δ 7.84–7.72 (br m, 0.5H), 7.59–7.48 (br m, 1H), 7.35–7.24 (m, 4H), 7.09 (d, J = 7.2 Hz, 1H), 6.82–6.74 (m, 0.5H), 6.73–6.65 (m, 0.5H), 5.21 (q, J = 7.3 Hz, 1H), 3.98–3.74 (br m, 2H), 3.56 (s, 3H), 3.19–3.10 (br m, 2H), 2.72–2.57 (m, 2H), 2.39 (br s, 3H), 1.64 (br m, 1H), 1.51 (br m, 2H), 1.09–0.93 (m, 2H). MS (ESI): m/z 433.2 [M + H]⁺.

(R)-3-((7-((S)-2-Amino-2-(2-methoxyphenyl)ethyl)amino)-5-methyl-[1,2,4]triazolo[1,5-a]pyrimidin-2-yl)amino)-3-(3-

chlorophenyl)propanenitrile (51). A yellow-orange mixture of **103** (41.7 mg, 0.120 mmol, 1.0 equiv) and **107a** (32 mg, 0.120 mmol, 1.0 equiv) in 1 mL of EtOH was treated with DIEA (0.105 mL, 0.601 mmol, 5.0 equiv) and allowed to heat at 70 °C overnight. The mixture was concentrated, dried briefly under high vacuum, and then dissolved in 1.5 mL of 2:1 CH₂Cl₂–TFA. The resulting light brown solution was allowed to stir at rt for 15 min, and then it was diluted with DCE and heptane, concentrated, and dried briefly under high vacuum. The residue was diluted with 1 mL of 1:1 MeCN–H₂O and filtered, the filter cake was rinsed once with 0.5 mL of 1:1 MeCN–H₂O, and the resulting solution was purified by RP-HPLC to give 45 mg of TFA salt of the desired product as a colorless powder. This material was dissolved in 1 mL of 1:1 MeCN–H₂O and filtered through a 100 mg Agilent StratoSpheres PL-HCO3MP SPE resin cartridge, the resin was rinsed with 1 mL of 1:1 MeCN–H₂O, and the filtrate was lyophilized to provide 25 mg (44%) of the free base of **51** as a colorless powder. ¹H NMR (400 MHz, CDCl₃) δ 7.47 (s, 1H), 7.42–7.28 (m, 5H), 7.05–6.97 (m, 1H), 6.94 (d, *J* = 8.2 Hz, 1H), 6.41 (s, 1H), 5.94 (s, 1H), 5.26–5.13 (m, 2H), 4.51 (s, 1H), 3.89 (s, 3H), 3.69–3.54 (m, 1H), 3.54–3.40 (m, 1H), 3.25–3.03 (m, 2H), 2.46 (s, 3H). HRMS (ESI): m/z 477.1921 [M + H]⁺.

*(R)-3-(3-Chlorophenyl)-3-((5-methyl-7-(4-methylpiperazin-1-yl)-1*H*-imidazo[4,5-*b*]pyridin-2-yl)amino)propanenitrile (55).* A mixture of **116** (85 mg, 0.152 mmol) in 2 mL of 1:1 toluene–TFA was stirred at rt for 3 h. The volatiles were evaporated, and the residue was partitioned between CH₂Cl₂ and saturated NaHCO₃. The layers were separated, and the aqueous layer was extracted twice more with CH₂Cl₂, and then the combined organic layers were washed with brine, dried over Na₂SO₄, and concentrated under reduced pressure. The crude material was dissolved in 1.5 mL of DMSO, filtered through a 0.45 μm syringe filter, and purified by SFC providing 21 mg (26%) of **55** as a pale yellow powder. ¹H NMR (500 MHz, CDCl₃) δ 7.44 (s, 1H), 7.36–7.32 (m, 1H), 7.32–7.29 (m, 2H), 6.18 (s, 1H), 5.56–5.38 (br m, 1H), 5.30–5.17 (m, 1H), 3.92–3.78 (br m, 4H), 3.20–3.09 (m, 2H), 2.61–2.55 (m, 4H), 2.47 (s, 3H), 2.36 (s, 3H). HRMS (ESI): m/z 410.1861 [M + H]⁺.

Using procedures analogous to those described for compound **55**, compound **56** was prepared.

*(R)-Methyl 4-(3-(2-Cyano-1-((5-methyl-7-(4-methylpiperazin-1-yl)-3*H*-imidazo[4,5-*b*]pyridin-2-yl)amino)ethyl)phenoxy)piperidine-1-carboxylate (56).* Ten mg (12%). ¹H NMR (400 MHz, CDCl₃) δ 7.34–7.29 (m, 1H), 7.09–7.02 (m, 2H), 6.93–6.86 (m, 1H), 6.23 (s, 1H), 5.20–5.10 (m, 1H), 4.58–4.47 (m, 1H), 3.92–3.77 (m, 4H), 3.71 (s, 5H), 3.48–3.35 (m, 3H), 3.15 (*t*, *J* = 5.3 Hz, 2H), 2.67–2.54 (m, 4H), 2.47 (s, 3H), 2.37 (s, 3H), 2.00–1.86 (m, 4H). MS (ESI): m/z 533.3 [M + H]⁺.

Methyl (R)-4-(3-((tert-Butoxycarbonyl)amino)-2-cyanoethyl)phenoxy)piperidine-1-carboxylate (73). A mixture of **64** (2.0 g, 7.62 mmol), methyl 4-((methylsulfonyl)oxy)piperidine-1-carboxylate (3.62 g, 15.25 mmol), and cesium carbonate (4.97 g, 15.25 mmol) in DMF (volume: 13.3 mL) was heated to 60 °C for 2 h and then at 80 °C for 3.5 h. LCMS at this time indicated complete consumption of starting phenol. The reaction mixture was diluted with water (50 mL) and extracted with EtOAc (3 × 50 mL). The combined organic extracts were washed with brine, dried over MgSO₄, and concentrated under reduced pressure to provide the crude material which was purified by a silica gel column chromatography eluting with a gradient of heptanes/ethyl acetate to give **73** (2 g, 4.96 mmol, 65% yield) as an off-white foam. MS (ESI): m/z 404.2 [M + H]⁺.

*Methyl 4-(3-((1R)-2-Cyano-1-((5-methyl-1-(tetrahydro-2H-pyran-2-yl)-1*H*-imidazo[4,5-*b*]pyridin-2-yl)amino)ethyl)phenoxy)piperidine-1-carboxylate (74).* Step 1: A hydrogen chloride solution (4 M in dioxane, 12 mL) was added to a solution of **73** (2 g, 4.96 mmol) in a 1:1 mixture of Et₂O/MeOH (100 mL). After stirring at rt for 2 h, the volatiles were removed under reduced pressure. The residue was treated with ethyl acetate (200 mL) and washed with saturated NaHCO₃ (100 mL). The organic layer was dried over MgSO₄, filtered, and evaporated under reduced pressure to provide the desired free amine (*R*)-methyl 4-(3-(1-amino-2-cyanoethyl)phenoxy)piperidine-1-carboxylate (584 mg, 1.93 mmol) as a colorless oil. ¹H

NMR ¹H NMR (400 MHz, DMSO-d₆) δ 7.23 (*t*, *J* = 7.7 Hz, 1H), 7.08–7.02 (m, 1H), 6.97 (dt, *J* = 7.6, 1.0 Hz, 1H), 6.86 (ddd, *J* = 8.3, 2.6, 0.9 Hz, 1H), 4.57 (tt, *J* = 7.8, 3.6 Hz, 1H), 4.10 (*t*, *J* = 6.4 Hz, 1H), 3.74–3.64 (m, 2H), 3.60 (s, 3H), 3.29–3.21 (m, 2H), 2.77 (dd, *J* = 6.4, 1.1 Hz, 2H), 1.97–1.87 (m, 2H), 1.54 (dtd, *J* = 12.4, 8.3, 3.8 Hz, 2H). MS (ESI): m/z 304.5 [M + H]⁺.

Step 2: **72** (1.8 g, 7.18 mmol), (*R*)-methyl 4-(3-(1-amino-2-cyanoethyl)phenoxy)piperidine-1-carboxylate (1.45 g, 4.79 mmol), tris(dibenzylideneacetone)dipalladium(0) (657 mg, 0.718 mmol), BINAP (894 mg, 1.436 mmol), and sodium *tert*-butoxide (644 mg, 6.70 mmol) were combined as a mixture in degassed toluene (20 mL) and heated to 85 °C for 16 h under N₂. The reaction mixture was cooled to rt and partitioned between saturated NH₄Cl (20 mL) and EtOAc (10 mL). Layers were separated, and the aqueous layer was extracted twice more with EtOAc (10 mL). The combined organic extracts were washed with brine, dried over MgSO₄, and concentrated under reduced pressure to give a yellow oil. SiO₂ flash chromatography (0 → 100% EtOAc/heptane) provided **74** (1.9 g, 3.66 mmol, 77% yield) as an off-white foam. LCMS indicated a 1:1 mixture of diastereomers. MS (ESI): m/z 519.5 [M + H]⁺.

*Benzyl (R)-4-(3-((tert-Butoxycarbonyl)amino)-2-cyanoethyl)-benzyl)-3,6-dihydro-1*H*-pyridine-1(2*H*)-carboxylate (83).* Intermediate **80** (300 mg, 0.88 mmol) was suspended in THF/water (3:1). Pinacol boronate **B** (364 mg, 1.06 mmol), Pd(PPh₃)₄ (102 mg, 0.088 mmol), and Cs₂CO₃ (864 mg, 2.65 mmol) were added, and the resulting suspension was heated to 120 °C in a microwave reactor for 30 min. Upon cooling to rt the mixture was filtered through Celite and concentrated under reduced pressure. SiO₂ flash chromatography (0 → 100% EtOAc/heptane) provided **83** (420 mg, quant). MS (ESI): m/z 420.2 [M-tBu+H]⁺.

*Methyl 4-(3-((1*R*)-2-Cyano-1-((5-methyl-1-(tetrahydro-2*H*-pyran-2-yl)-1*H*-imidazo[4,5-*b*]pyridin-2-yl)amino)ethyl)benzyl)piperidine-1-carboxylate (84).* Step 1: Intermediate **83** (420 mg, 0.88 mmol) was suspended in EtOAc (10 mL), and 10% Pd/C (188 mg, 0.18 mmol) was added. The resulting suspension was stirred under an atmosphere of hydrogen for 5 h resulting in hydrogenolysis of the Cbz group and hydrogenation of the piperidine olefin. The mixture was filtered through Celite, and solvent was evaporated under reduced pressure to give *tert*-butyl (*R*)-(2-cyano-1-(3-(piperidin-4-ylmethyl)phenyl)ethyl)carbamate which was used without further purification. MS (ESI): m/z 344.3 [M + H]⁺. Step 2: Methyl chloroformate (113 μL, 1.46 mmol) was added to a suspension of *tert*-butyl (*R*)-(2-cyano-1-(3-(piperidin-4-ylmethyl)phenyl)ethyl)carbamate (100 mg, 0.29 mmol) in THF (1 mL). After stirring for 15 min at rt the mixture was concentrated under reduced pressure, and the crude residue was subjected to SiO₂ flash chromatography (0 → 100% EtOAc/heptane) to give methyl (*R*)-4-(3-((*tert*-butoxycarbonyl)amino)-2-cyanoethyl)benzyl)piperidine-1-carboxylate (110 mg, 94%). MS (ESI): m/z 346.3 [M-tBu+H]⁺. Step 3: A suspension of (*R*)-4-(3-((*tert*-butoxycarbonyl)amino)-2-cyanoethyl)benzyl)piperidine-1-carboxylate (40 mg, 0.1 mmol) in 1,1,3,3,3-hexafluoroisopropanol was heated to 150 °C for 20 min in a microwave reactor. Upon cooling to rt volatiles were evaporated under reduced pressure to give methyl (*R*)-4-(3-(1-amino-2-cyanoethyl)benzyl)piperidine-1-carboxylate which was used immediately in the next step without purification. MS (ESI): m/z 302.2 [M + H]⁺. Step 4: methyl (*R*)-4-(3-(1-amino-2-cyanoethyl)benzyl)piperidine-1-carboxylate (32 mg, 0.11 mmol) was combined with intermediate **72** (37 mg, 0.15 mmol), tris(dibenzylideneacetone)dipalladium(0) (9.7 mg, 10.6 μmol), BINAP (13.2 mg, 21 μmol), and sodium *tert*-butoxide (14.2 mg, 0.15 mmol) in a 5 mL microwave vessel. The vessel was evacuated and flushed with nitrogen. Degassed toluene (8 mL) was then added. The resulting mixture was heated to 85 °C for 16 h. The reaction mixture was cooled to rt and partitioned between water (25 mL), brine (~25 mL), and EtOAc (25 mL). Layers were separated, and the aqueous layer was extracted twice more with EtOAc (25 mL). The combined organic extracts were washed with brine, dried over MgSO₄, and concentrated under reduced pressure. SiO₂ flash chromatography (0 → 100% EtOAc/heptane then 0 → 40% MeOH/DCM) gave **84** contaminated with BINAP-derived side products (55 mg). MS (ESI): m/z 517.3 [M + H]⁺.

tert-Butyl (S)-(2-Hydroxy-1-(2-methoxyphenyl)ethyl)carbamate (106a). Red-Al (65% in toluene, 1 mL, 3.33 mmol, 3.33 equiv) was allowed to cool to 0 °C, then a colorless solution of **104a** (281 mg, 0.999 mmol) in 1 mL of THF was added dropwise over 5–10 min (gas evolution), followed by a rinse with 0.5 mL of THF. The pale yellow mixture was allowed to stir at 0 °C for 3 h. The reaction was quenched with 250 μL of MeOH (vigorous gas evolution), followed by 4 g of 50 wt % aq. potassium sodium tartrate tetrahydrate (gas evolution). The resulting mixture was allowed to warm to rt and stirred well at that temperature for 30 min to give three phases. The bottom phase was removed and extracted 3 × 2 mL of EtOAc. The EtOAc extracts were combined with the remaining top two phases from the initial triphasic solution and then washed twice with 1:1 saturated NaHCO₃–water and once with brine. The organic layer was dried with MgSO₄, filtered, and evaporated to give 252 mg (94%) of **106a** as a yellow solid, which was taken on without further purification. ¹H NMR (400 MHz, CDCl₃) δ 7.30–7.24 (m, 1H), 7.23 (dd, *J* = 7.5, 1.5 Hz, 1H), 6.98–6.92 (m, 1H), 6.89 (d, *J* = 8.2 Hz, 1H), 5.54 (s, 1H), 5.05 (s, 1H), 3.85 (s, 3H), 3.84–3.75 (m, 2H), 1.44 (s, 9H). MS (ESI): *m/z* 268.2 [M + H]⁺.

tert-Butyl (S)-(2-Amino-1-(2-methoxyphenyl)ethyl)carbamate (107a). **Step 1:** A solution of **106a** (252 mg, 0.943 mmol, 1.0 equiv) in 3 mL of CH₂Cl₂ was treated with Et₃N (0.208 mL, 1.498 mmol, 1.6 equiv) and allowed to cool to 0 °C before MsCl (0.093 mL, 1.199 mmol, 1.27 equiv) was added dropwise over a couple of minutes. The resulting pale yellow mixture was allowed to stir at 0 °C for 30 min, and then the mixture was quenched with saturated NH₄Cl and diluted with 10 mL of EtOAc. The aqueous layer was removed, and then the organic layer was washed once with brine, dried with MgSO₄, filtered, and concentrated to give 330 mg (quant.) of crude (S)-2-((*tert*-butoxycarbonyl)amino)-2-(2-methoxyphenyl)-ethylmethanesulfonate as a pale yellow solid, which was taken on without further purification. **Step 2:** A light yellow mixture of crude (S)-2-((*tert*-butoxycarbonyl)amino)-2-(2-methoxyphenyl)-ethylmethanesulfonate (330 mg, 0.943 mmol, 1.0 equiv) and NaN₃ (260 mg, 4.00 mmol, 4.24 equiv) in 2 mL of DMF was allowed to stir well at 60 °C overnight. After allowing the mixture to cool to rt and adding 10 mL of EtOAc, the mixture was diluted to ~20 mL total volume with water. The aqueous layer was removed, and then the organic layer was washed twice with water, once with brine, dried with MgSO₄, filtered, and dry loaded onto SiO₂. The material was purified by silica gel flash column chromatography (0 → 50% EtOAc/heptane) to provide 86 mg (31%) of *tert*-butyl (S)-(2-azido-1-(2-methoxyphenyl)ethyl)carbamate as a colorless solid. ¹H NMR (400 MHz, CDCl₃) δ 7.33–7.28 (m, 1H), 7.23 (d, *J* = 7.5 Hz, 1H), 6.96 (t, *J* = 7.4 Hz, 1H), 6.90 (d, *J* = 8.2 Hz, 1H), 5.50 (s, 1H), 5.08 (s, 1H), 3.88 (s, 3H), 3.56 (qd, *J* = 12.1, 6.7 Hz, 2H), 1.44 (s, 9H). MS (ESI): *m/z* 293.3 [M + H]⁺. **Step 3:** A solution of (S)-*tert*-butyl (2-azido-1-(2-methoxyphenyl)ethyl)carbamate (86 mg, 0.294 mmol, 1.0 equiv) in 2 mL of EtOH was treated with 10% Pd/C (50% water, 62.6 mg, 0.029 mmol, 0.1 equiv), and then hydrogen was bubbled through the dark mixture for ~5 min before the reaction was allowed to stir well at rt under a balloon of hydrogen for 15 min. The mixture was sparged with nitrogen, dried with MgSO₄, filtered, and concentrated to give 64 mg (82%) of **107a** as a colorless solid, which was taken on without further purification. ¹H NMR (500 MHz, CDCl₃) δ 7.25–7.15 (m, 2H), 6.97–6.80 (m, 2H), 5.61 (br s, 1H), 4.83 (br s, 1H), 3.85 (s, 3H), 2.94 (p, *J* = 7.1, 6.5 Hz, 2H), 1.43 (s, 9H). MS (ESI): *m/z* 267.3 [M + H]⁺.

N-(2,4-Dimethoxybenzyl)-6-methyl-4-(4-methylpiperazin-1-yl)-3-nitropyridin-2-amine (113). A brown solution of **112** (15 g, 72.5 mmol, 1.0 equiv) and Et₃N (30.3 mL, 217 mmol, 3.0 equiv) in 181 mL of EtOH was treated with 1-methylpiperazine (8.04 mL, 72.5 mmol, 1.0 equiv) and allowed to stir at room temperature for 3.5 h. 2,4-Dimethoxybenzylamine (16.33 mL, 109 mmol, 1.5 equiv) was then added, and the mixture was heated at reflux overnight. The volatiles were evaporated under reduced pressure, and the residue was suspended in 400 mL of EtOAc and washed with water and brine, then dried over MgSO₄, and concentrated under reduced pressure. The residue was purified by silica gel flash column chromatography (0 → 10% i-PrOH/CH₂Cl₂) to provide 15 g (52%) of **113** as a dark

orange oil. ¹H NMR (400 MHz, CDCl₃) δ 8.25 (t, *J* = 5.6 Hz, 1H), 6.47 (d, *J* = 2.4 Hz, 1H), 6.42 (dd, *J* = 8.2, 2.4 Hz, 1H), 5.95 (s, 1H), 4.68 (d, *J* = 5.6 Hz, 2H), 3.86 (s, 3H), 3.79 (s, 3H), 3.24–3.13 (m, 4H), 2.56–2.48 (m, 4H), 2.36–2.29 (m, 6H). MS (ESI): *m/z* 402.4 [M + H]⁺.

3-(2,4-Dimethoxybenzyl)-5-methyl-7-(4-methylpiperazin-1-yl)-3H-imidazo[4,5-b]pyridine (114). An orange solution of **113** (15 g, 37.4 mmol, 1.0 equiv) in 250 mL of 1:1 THF–MeOH was treated with Zn powder (12.21 g, 187 mmol, 5.0 equiv) and allowed to cool to 0 °C before 125 mL of saturated aqueous NH₄Cl was added dropwise via addition funnel with vigorous stirring. The resulting mixture was allowed to stir well at 0 °C for 15 min and then allowed to warm to rt and stir for 90 min, at which time an additional ~1 g of Zn and 25 mL of saturated NH₄Cl were added. After 2.5 h, saturated aqueous NaHCO₃ (300 mL) was added, the mixture was filtered through Celite, and the filter cake was rinsed with 250 mL of EtOAc. The aqueous layer was separated and extracted with EtOAc (2 × 150 mL), and then the combined organic layers were washed with brine and dried over MgSO₄ before being concentrated under reduced pressure to give N²-(2,4-dimethoxybenzyl)-6-methyl-4-(4-methylpiperazin-1-yl)pyridine-2,3-diamine as a brown oil. ¹H NMR (500 MHz, CDCl₃) δ 7.32 (d, *J* = 8.3 Hz, 1H), 6.48 (d, *J* = 2.4 Hz, 1H), 6.44 (dd, *J* = 8.1, 2.4 Hz, 1H), 6.29 (s, 1H), 4.53 (d, *J* = 4.9 Hz, 2H), 4.33 (s, 1H), 3.84 (s, 3H), 3.80 (s, 3H), 3.31 (s, 2H), 2.93 (s, 4H), 2.57 (s, 4H), 2.37 (s, 3H), 2.36 (s, 3H). MS (ESI): *m/z* 372.4 [M + H]⁺. A mixture of crude N²-(2,4-dimethoxybenzyl)-6-methyl-4-(4-methylpiperazin-1-yl)pyridine-2,3-diamine and *p*-TsOH·H₂O (0.702 g, 3.69 mmol, 0.1 equiv) in 369 mL of trimethyl orthoformate was heated to 100 °C for 30 min. The reaction mixture was diluted with 500 mL of EtOAc and washed sequentially with 250 mL each of saturated NaHCO₃ and brine, then dried over MgSO₄, and concentrated under reduced pressure. The resulting brown solid was suspended in EtOAc. Heptane was added, and the beige solid was collected by suction filtration. The filtrate was concentrated and triturated again to yield a total of 8.7 g (62%) of **114** as a dark gray solid. ¹H NMR (400 MHz, CDCl₃) δ 7.73 (s, 1H), 7.20 (d, *J* = 8.3 Hz, 1H), 6.45 (d, *J* = 2.4 Hz, 1H), 6.40 (dd, *J* = 8.3, 2.4 Hz, 1H), 6.31 (s, 1H), 5.30 (s, 2H), 3.91–3.85 (m, 4H), 3.82 (s, 3H), 3.77 (s, 3H), 2.62–2.57 (m, 4H), 2.55 (s, 3H), 2.35 (s, 3H). MS (ESI): *m/z* 382.4 [M + H]⁺.

2-Bromo-3-(2,4-dimethoxybenzyl)-5-methyl-7-(4-methylpiperazin-1-yl)-3H-imidazo[4,5-b]pyridine (115). A solution of **114** (8.7 g, 22.81 mmol, 1.0 equiv) in 228 mL of THF at –40 °C was treated with *n*-butyllithium (2.5 M in hexanes, 10.95 mL, 27.4 mmol, 1.2 equiv) dropwise. The mixture became green and was stirred at –40 °C for 30 min before a solution of CBr₄ (11.34 g, 34.2 mmol, 1.5 equiv) in 30 mL of THF was added. The mixture became dark brown and was warmed slowly to 0 °C over ~2 h. The reaction was quenched with 200 mL of saturated aqueous NH₄Cl, and then 200 mL of water was added to dissolve the solids. The mixture was extracted with CHCl₃ (3 × 150 mL), and the combined organic extracts were washed with brine, dried over MgSO₄, and concentrated under reduced pressure. The residue was purified by silica gel flash column chromatography (CH₂Cl₂ → 10:89.5:0.5 MeOH–CH₂Cl₂–Et₃N) to provide 6.3 g (60%) of **115** as a brown solid. ¹H NMR (400 MHz, CDCl₃) δ 6.58 (d, *J* = 8.4 Hz, 1H), 6.45 (d, *J* = 2.4 Hz, 1H), 6.32–6.27 (m, 2H), 5.38 (d, *J* = 0.9 Hz, 2H), 3.91–3.82 (m, 7H), 3.75 (s, 3H), 2.64–2.59 (m, 4H), 2.48 (s, 3H), 2.37 (s, 3H). MS (ESI): *m/z* 460.3 [M + H]⁺.

(R)-3-(3-Chlorophenyl)-3-((3-(2,4-dimethoxybenzyl)-5-methyl-7-(4-methylpiperazin-1-yl)-3H-imidazo[4,5-b]pyridin-2-yl)amino)propanenitrile (116). A 2 mL microwave vessel containing a mixture of **115** (100 mg, 0.217 mmol, 1.0 equiv), amine G (47.1 mg, 0.261 mmol, 1.2 equiv), Pd₂dba₃ (19.89 mg, 0.022 mmol, 0.1 equiv), BINAP (40.6 mg, 0.065 mmol, 0.3 equiv), and sodium *tert*-butoxide (25.05 mg, 0.261 mmol, 1.2 equiv) was evacuated and refilled with nitrogen, and then 2.2 mL of degassed toluene was added. The resulting mixture was heated to 85 °C for 4.5 h. The mixture was diluted with water and extracted with EtOAc three times, and then the combined organic extracts were washed with brine, dried over Na₂SO₄, and concentrated under reduced pressure. The residue was purified by silica gel flash column chromatography (CH₂Cl₂ → 10:90:0.25 MeOH–CH₂Cl₂

DIEA) to provide 85 mg (70%) of **116** that was contaminated by remaining **115**. This mixture was submitted directly to deprotection. MS (ESI): *m/z* 560.2 [M + H]⁺.

■ ASSOCIATED CONTENT

Supporting Information

The Supporting Information is available free of charge on the ACS Publications website at DOI: [10.1021/acs.jmedchem.7b01861](https://doi.org/10.1021/acs.jmedchem.7b01861).

Experimental procedures describing general experimental information, preparation of chemical intermediates, procedures for generating genetic strains and resistant strains, crystallographic methods and references, and a complete listing of SPR data ([PDF](#))

X-ray crystallographic and structure refinement statistics ([PDF](#))

Molecular formula strings ([CSV](#))

Accession Codes

Structural coordinates have been deposited in the RCSB Protein Data Bank under the accession codes 6CHL (**3**), 6CHM (**5**), 6CHO (**7**), 6CHN (**9**), 6CHP (**11**), 6CHQ (**28**), and 6CKW (**51**). Authors will release the atomic coordinates and experimental data upon article publication.

■ AUTHOR INFORMATION

Corresponding Author

*Phone: +1 510 879 9317. E-mail: colin.skepper@novartis.com.

ORCID

Colin K. Skepper: [0000-0002-6771-2024](https://orcid.org/0000-0002-6771-2024)

Robert J. Moreau: [0000-0002-9056-7128](https://orcid.org/0000-0002-9056-7128)

Brian Y. Feng: [0000-0002-4208-8624](https://orcid.org/0000-0002-4208-8624)

Andreas Lingel: [0000-0003-2909-4920](https://orcid.org/0000-0003-2909-4920)

Author Contributions

The manuscript was written through contributions of all authors. All authors have given approval to the final version of the manuscript.

Notes

The authors declare no competing financial interest.

■ ACKNOWLEDGMENTS

This work was funded by Novartis AG. The authors thank Shengtian Yang for NMR structure elucidation support and Weiping Jia, Heidi Struble, Dazhi Tang, Alice Wan Wang, and Da Wang for analytical support.

■ ABBREVIATIONS USED

FBLD, fragment-based lead discovery; PPAT, phosphopantetheine adenyl transferase; SPR, surface plasmon resonance; tPSA, topological polar surface area

■ REFERENCES

- (1) (a) Neu, H. C. The crisis in antibiotic resistance. *Science* **1992**, *257*, 1064–1073. (b) Alanis, A. J. Resistance to antibiotics: are we in the post-antibiotic era? *Arch. Med. Res.* **2005**, *36*, 697–705. (c) Levy, S. B.; Marshall, B. Antibacterial resistance worldwide: causes, challenges and responses. *Nat. Med.* **2004**, *10*, S122–S129. (d) Ventola, C. L. The antibiotic resistance crisis. Part 1: causes and threats. *PT* **2015**, *40*, 277–283. (e) Hwang, A. Y.; Gums, J. G. The emergence and evolution of antimicrobial resistance: impact on a global scale. *Bioorg. Med. Chem.* **2016**, *24*, 6440–6445.
- (2) (a) Centers for Disease Control and Prevention. Antibiotic Resistance Threats in the United States, 2013. <http://www.cdc.gov/drugresistance/threat-report-2013/> (accessed Mar 14, 2018). (b) World Health Organization. Antimicrobial Resistance: Global Report on Surveillance 2014. <http://www.who.int/drugresistance/documents/surveillancereport/en/> (accessed Mar 14, 2018).
- (3) (a) Overbye, K. M.; Barrett, J. F. Antibiotics: where did we go wrong? *Drug Discovery Today* **2005**, *10* (1), 45–52. (b) Spellberg, B.; Guidos, R.; Gilbert, D.; Bradley, J.; Boucher, H. W.; Scheld, W. M.; Bartlett, J. G.; Edwards, J., Jr. The epidemic of antibiotic-resistant infections: a call to action for the medical community from the Infectious Diseases Society of America. *Clin. Infect. Dis.* **2008**, *46*, 155–164. (c) Rice, L. B. Federal funding for the study of antimicrobial resistance in nosocomial pathogens: no ESKAPE. *J. Infect. Dis.* **2008**, *197*, 1079–1081.
- (4) Fischbach, M. A.; Walsh, C. T. Antibiotics for emerging pathogens. *Science* **2009**, *325*, 1089–1093.
- (5) (a) Walsh, C. Molecular mechanisms that confer antibacterial drug resistance. *Nature* **2000**, *406*, 775–781. (b) Alekshun, M. N.; Levy, S. B. Molecular mechanisms of antibacterial multidrug resistance. *Cell* **2007**, *128*, 1037–1050. (c) Nikaido, H. Multidrug resistance in bacteria. *Annu. Rev. Biochem.* **2009**, *78*, 119–146. (d) Rice, L. B. Mechanisms of resistance and clinical relevance of resistance to β -lactams, glycopeptides, and fluoroquinolones. *Mayo Clin. Proc.* **2012**, *87* (2), 198–208. (f) Blair, J. M. A.; Webber, M. A.; Baylay, A. J.; Ogbolu, D. O.; Piddock, L. J. V. Molecular mechanisms of antibiotic resistance. *Nat. Rev. Microbiol.* **2015**, *13*, 42–51.
- (6) (a) Liu, Y. – Y.; Wang, Y.; Walsh, T. R.; Yi, L. – X.; Zhang, R.; Spencer, J.; Doi, Y.; Tian, G.; Dong, B.; Huang, X.; Yu, L. – F.; Gu, D.; Ren, H.; Chen, X.; Lv, L.; He, D.; Zhou, H.; Liang, Z.; Liu, J. – H.; Shen, J. Emergence of plasmid-mediated colistin resistance mechanism MCR-1 in animals and human beings in China: a microbiological and molecular biological study. *Lancet Infect. Dis.* **2016**, *16*, 161–168. (b) Hasman, H.; Hammerum, A. M.; Hansen, F.; Hendriksen, R. S.; Olesen, B.; Agersø, Y.; Zankari, E.; Leekitcharoenphon, P.; Stegger, M.; Kaas, R. S.; Cavaco, L. M.; Hansen, D. S.; Aarestrup, F. M.; Skov, R. L. Detection of mcr-1 encoding plasmid-mediated colistin-resistant *Escherichia coli* isolates from human bloodstream infection and imported chicken meat, Denmark 2015. *Eurosurveillance (Online Edition)* **2015**, *20*, 1–5. (c) Falgenhauer, L.; Waezsada, S. E.; Yao, Y.; Imirzalioglu, C.; Käsbohrer, A.; Roesler, U.; Michael, G. B.; Schwarz, S.; Werner, G.; Kreienbrock, L.; Chakraborty, T. Colistin resistance gene mcr-1 in extended-spectrum β -lactamase-producing and carbapenemase-producing gram-negative bacteria in Germany. *Lancet Infect. Dis.* **2016**, *16*, 282–283. (d) Malhotra-Kumar, S.; Xavier, B. B.; Das, A. J.; Lammens, C.; Hoang, H. T. T.; Pham, N. T.; Goossens, H. Colistin-resistant *Escherichia coli* harbouring mcr-1 isolated from food animals in Hanoi, Vietnam. *Lancet Infect. Dis.* **2016**, *16*, 286–287. (e) Quesada, A.; Ugarte-Ruiz, M.; Iglesias, M. R.; Porrero, M. C.; Martínez, R.; Florez-Cuadrado, D.; Campos, M. J.; García, M.; Píriz, S.; Sáez, J. L.; Domínguez, L. Detection of plasmid mediated colistin resistance (MCR-1) in *Escherichia coli* and *Salmonella enterica* isolated from poultry and swine in Spain. *Res. Vet. Sci.* **2016**, *105*, 134–135. (f) U.S. Department of Health and Human Services (HHS). Proactive Efforts by U.S. Federal Agencies Enable Early Detection of New Antibiotic Resistance, 2016. <https://wayback.archive-it.org/8315/20170119094421/https://www.hhs.gov/blog/2016/05/26/early-detection-new-antibiotic-resistance.html> (accessed Mar 14, 2018).
- (7) Chen, L.; Todd, R.; Kiehlbauch, J.; Walters, M.; Kallen, A. Notes from the field: pan-resistant New Delhi metallo-beta-lactamase-producing *Klebsiella pneumoniae* - Washoe County, Nevada, 2016. *MMWR Morb. Mortal. Wkly Rep.* **2017**, *66* (1), 33.
- (8) (a) Nikaido, H. Prevention of drug access to bacterial targets: permeability barriers and active efflux. *Science* **1994**, *264*, 382–387. (b) Nikaido, H. Multidrug efflux pumps of gram-negative bacteria. *J. Bacteriol.* **1996**, *178*, 5853–5859. (c) Hancock, R. E. W. The bacterial outer membrane as a drug barrier. *Trends Microbiol.* **1997**, *5* (1), 37–42. (d) Nikaido, H. Molecular basis of bacterial outer membrane

- permeability revisited. *Microbiol. Mol. Biol. R.* **2003**, *67* (4), 593–656. (e) Li, X. – Z.; Nikaido, H. Efflux-mediated drug resistance in bacteria. *Drugs* **2004**, *64* (2), 159–204. (f) Kumar, A.; Schweizer, H. P. Bacterial resistance to antibiotics: active efflux and reduced uptake. *Adv. Drug Delivery Rev.* **2005**, *57*, 1486–1513. (g) Lomovskaya, O.; Zgurskaya, H. I.; Totrov, M.; Watkins, W. J. Waltzing transporters and ‘the dance macabre’ between humans and bacteria. *Nat. Rev. Drug Discovery* **2007**, *6*, 56–65. (h) Delcour, A. H. Outer membrane permeability and antibiotic resistance. *Biochim. Biophys. Acta, Proteins Proteomics* **2009**, *1794*, 808–816. (i) Manchester, J. I.; Buurman, E. T.; Bisacchi, G. S.; McLaughlin, R. E. Molecular determinants of AcrB-mediated bacterial efflux: implications for drug discovery. *J. Med. Chem.* **2012**, *55*, 2532–2537. (j) Zgurskaya, H.; López, C. A.; Gnanakaran, S. Permeability barrier of gram-negative cell envelopes and approaches to bypass it. *ACS Infect. Dis.* **2015**, *1* (11), 512–522. (k) Silver, L. L. A gestalt approach to gram-negative entry. *Bioorg. Med. Chem.* **2016**, *24*, 6379–6389.
- (9) (a) O’Shea, R.; Moser, H. E. Physicochemical properties of antibacterial compounds: implications for drug discovery. *J. Med. Chem.* **2008**, *51*, 2871–2878. (b) Payne, D. J.; Gwynn, M. N.; Holmes, D. J.; Pompili, D. L. Drugs for bad bugs: confronting the challenges of antibacterial discovery. *Nat. Rev. Drug Discovery* **2007**, *6*, 29–40. (c) Silver, L. L. Challenges of antibacterial discovery. *Clin. Microbiol. Rev.* **2011**, *24* (1), 71–109. (d) Brown, D. G.; May-Dracka, T. L.; Gagnon, M. M.; Tommasi, R. Trends and exceptions of physical properties on antibacterial activity for gram-positive and gram-negative pathogens. *J. Med. Chem.* **2014**, *57*, 10144–10161. (e) Tommasi, R.; Brown, D. G.; Walkup, G. K.; Manchester, J. I.; Miller, A. A. ESKAPEing the labyrinth of antibacterial drug discovery. *Nat. Rev. Drug Discovery* **2015**, *14*, 529–542.
- (10) Leonardi, R.; Zhang, Y. M.; Rock, C. O.; Jackowski, S. Coenzyme A: back in action. *Prog. Lipid Res.* **2005**, *44*, 125–153.
- (11) (a) Harrington, C. R.; Baddiley, J. Biosynthesis of wall teichoic acids in *Staphylococcus aureus* H, *Micrococcus varians* and *Bacillus subtilis* W23. *Eur. J. Biochem.* **1985**, *153*, 639–645. (b) Zhang, Y. – M.; Rock, C. O. Membrane lipid homeostasis in bacteria. *Nat. Rev. Microbiol.* **2008**, *6*, 222–233.
- (12) (a) Anderson, M. S.; Bulawa, C. E.; Raetz, C. R. H. The biosynthesis of gram-negative endotoxin. Formation of lipid A precursors from UDP-GlcNAc in extracts of *Escherichia coli*. *J. Biol. Chem.* **1985**, *260*, 15536–15541. (b) Brozek, K. A.; Raetz, C. R. H. Biosynthesis of lipid A in *Escherichia coli*. Acyl carrier protein-dependent incorporation of laurate and myristate. *J. Biol. Chem.* **1990**, *265*, 15410–15417. (c) Masoudi, A.; Raetz, C. R. H.; Zhou, P.; Pemble, C. W., IV Chasing acyl carrier protein through a catalytic cycle of lipid A production. *Nature* **2014**, *505*, 422–426.
- (13) Begley, T. P.; Kinsland, C.; Strauss, E. The biosynthesis of coenzyme A in bacteria. *Vitam. Horm.* **2001**, *61*, 157–171.
- (14) (a) Geerlof, A.; Lewendon, A.; Shaw, W. V. Purification and characterization of phosphopantetheine adenylyltransferase from *Escherichia coli*. *J. Biol. Chem.* **1999**, *274*, 27105–27111. (b) Izard, T. The crystal structures of phosphopantetheine adenylyltransferase with bound substrates reveal the enzyme’s catalytic mechanism. *J. Mol. Biol.* **2002**, *315*, 487–495.
- (15) (a) Gerdes, S. Y.; Scholle, M. D.; D’Souza, M.; Bernal, A.; Baev, M. V.; Farrell, M.; Kurnasov, O. V.; Daugherty, M. D.; Mseeh, F.; Polanuyer, B. M.; Campbell, J. W.; Anantha, S.; Shatalin, K. Y.; Chowdhury, S. A. K.; Fonstein, M. Y.; Osterman, A. L. From genetic footprinting to antimicrobial drug targets: examples in cofactor biosynthetic pathways. *J. Bacteriol.* **2002**, *184*, 4555–4572. (b) Genschel, U. Coenzyme A biosynthesis: reconstruction of the pathway in archaea and an evolutionary scenario based on comparative genomics. *Mol. Biol. Evol.* **2004**, *21*, 1242–1251.
- (16) Daugherty, M.; Polanuyer, B.; Farrell, M.; Scholle, M.; Lykidis, A.; de Crécy-Lagard, V.; Osterman, A. Complete reconstitution of the human coenzyme A biosynthetic pathway via comparative genomics. *J. Biol. Chem.* **2002**, *277*, 21431–21439.
- (17) Zhao, L.; Allanson, N. M.; Thomson, S. P.; Maclean, J. K. F.; Barker, J. J.; Primrose, W. U.; Tyler, P. D.; Lewendon, A. Inhibitors of phosphopantetheine adenylyltransferase. *Eur. J. Med. Chem.* **2003**, *38*, 345–349.
- (18) de Jonge, B. L. M.; Walkup, G. K.; Lahiri, S. D.; Huynh, H.; Neckermann, G.; Utley, L.; Nash, T. J.; Brock, J.; San Martin, M.; Kutschke, A.; Johnstone, M.; Laganas, V.; Hajec, L.; Gu, R.-F.; Ni, H.; Chen, B.; Hutchings, K.; Holt, E.; McKinney, D.; Gao, N.; Livchak, S.; Thresher, J. Discovery of inhibitors of 4'-phosphopantetheine adenylyltransferase (PPAT) to validate PPAT as a target for antibacterial therapy. *Antimicrob. Agents Chemother.* **2013**, *57*, 6005–6015.
- (19) Moreau, R. J.; Skepper, C. K.; Appleton, B. A.; Blechschmidt, A.; Balibar, C. J.; Benton, B. M.; Drumm, J. E.; Feng, B. Y.; Geng, M.; Li, C.; Lindvall, M. K.; Lingel, A.; Lu, Y.; Mamo, M.; Mergo, W.; Polyakov, V.; Smith, T. M.; Takeoka, K.; Uehara, K.; Wang, L.; Wei, J. – R.; Weiss, A. H.; Xie, L.; Xu, W.; Zhang, Q.; de Vicente, J. Fragment-based drug discovery of inhibitors of phosphopantetheine adenylyltransferase from gram-negative bacteria. *J. Med. Chem.* **2018**, DOI: [10.1021/acs.jmedchem.7b01691](https://doi.org/10.1021/acs.jmedchem.7b01691).
- (20) (a) Clackson, T.; Wells, J. A. A hot spot of binding energy in a hormone-receptor interface. *Science* **1995**, *267*, 383–386. (b) DeLano, W. L. Unraveling hot spots in binding interfaces: progress and challenges. *Curr. Opin. Struct. Biol.* **2002**, *12*, 14–20. (c) Hall, D. R.; Kozakov, D.; Whitty, A.; Vajda, S. Lessons from hot spot analysis for fragment-based drug discovery. *Trends Pharmacol. Sci.* **2015**, *36*, 724–736.
- (21) Average measured $pK_a = 6.6$ across multiple analogs.
- (22) Brameld, K. A.; Kuhn, B.; Reuter, D. C.; Stahl, M. Small molecule conformational preferences derived from crystal structure data. A medicinal chemistry focused analysis. *J. Chem. Inf. Model.* **2008**, *48*, 1–24.
- (23) Rath, C. M.; Benton, B. M.; de Vicente, J.; Drumm, J. E.; Geng, M.; Li, C.; Moreau, R.; Shen, X.; Skepper, C. K.; Steffek, M.; Takeoka, K.; Wang, L.; Wei, J. – R.; Xu, W.; Zhang, Q.; Feng, B. Optimization of CoAD inhibitors against gram-negative organisms through targeted metabolomics. *ACS Infect. Dis.* **2018**, *4*, 391–402.
- (24) The improvement in biochemical and cellular potency may be greater, but measurement was limited by the lower bounds of the respective assays.
- (25) McGaughey, G. B.; Gagné, M.; Rappé, A. K. π -Stacking interactions. Alive and well in proteins. *J. Biol. Chem.* **1998**, *273*, 15458–15463.
- (26) (a) Ma, D.; Cook, D. N.; Alberti, M.; Pon, N. G.; Nikaido, H.; Hearst, J. E. Genes *acrA* and *acrB* encode a stress-induced efflux system of *Escherichia coli*. *Mol. Microbiol.* **1995**, *16*, 45–55. (b) Fralick, J. A. Evidence that TolC is required for functioning of the Mar/AcrAB efflux pump of *Escherichia coli*. *J. Bacteriol.* **1996**, *178*, 5803–5805. (c) Zgurskaya, H. I.; Krishnamoorthy, G.; Ntreh, A.; Lu, S. Mechanism and function of the outer membrane channel TolC in multidrug resistance and physiology of enterobacteria. *Front. Microbiol.* **2011**, *2*, 1–13.
- (27) (a) Sampson, B. A.; Misra, R.; Benson, S. A. Identification and characterization of a new gene of *Escherichia coli* K-12 involved in outer membrane permeability. *Genetics* **1989**, *122*, 491–501. (b) Bos, M. P.; Tefsen, B.; Geurtzen, J.; Tommassen, J. Identification of an outer membrane protein required for the transport of lipopolysaccharide to the bacterial cell surface. *Proc. Natl. Acad. Sci. U. S. A.* **2004**, *101*, 9417–9422.
- (28) At 8-fold the MIC no resistant colonies were isolated. See: Fung-Tomc, J.; Gradel斯基, E.; Huczko, E.; Minassian, B.; Bonner, D. P. Activity of gatifloxacin against strains resistant to ofloxacin and ciprofloxacin and its ability to select for less susceptible bacterial variants. *Int. J. Antimicrob. Agents* **2001**, *18*, 77–80.
- (29) (a) Chan, D. M. T.; Monaco, K. L.; Wang, R.-P.; Winters, M. P. New N- and O-arylations with phenylboronic acids and cupric acetate. *Tetrahedron Lett.* **1998**, *39*, 2933–2936. (b) Evans, D. A.; Katz, J. L.; West, T. R. Synthesis of diaryl ethers through the copper-promoted arylation of phenols with arylboronic acids. An expedient synthesis of thyroxine. *Tetrahedron Lett.* **1998**, *39*, 2937–2940. (c) Lam, P. Y. S.; Clark, C. G.; Saubern, S.; Adams, J.; Winters, M. P.; Chan, D. M. T.;

- Combs, A. New aryl/heteroaryl C–N bond cross-coupling reactions via arylboronic acid/cupric acetate arylation. *Tetrahedron Lett.* **1998**, *39*, 2941–2944.
- (30) (a) Liu, G.; Cogan, D. A.; Ellman, J. A. Catalytic asymmetric synthesis of *tert*-butanesulfonamide. Application to the asymmetric synthesis of amines. *J. Am. Chem. Soc.* **1997**, *119*, 9913–9914. (b) Tang, T. P.; Ellman, J. A. Asymmetric synthesis of β -amino acid derivatives incorporating a broad range of substitution patterns by enolate additions to *tert*-butanesulfinyl imines. *J. Org. Chem.* **2002**, *67*, 7819–7832. (c) Robak, M. T.; Herbage, M. A.; Ellman, J. A. Synthesis and applications of *tert*-butanesulfonamide. *Chem. Rev.* **2010**, *110*, 3600–3740. (d) Chandrasekhar, S.; Pendke, M.; Muththe, C.; Akondi, S. M.; Mainkar, P. S. Synthesis of α,α -dideutero- β -amino esters. *Tetrahedron Lett.* **2012**, *S3*, 1292–1295.
- (31) Anderson, K. W.; Ikawa, T.; Tundel, R. E.; Buchwald, S. L. The selective reaction of aryl halides with KOH: synthesis of phenols, aromatic ethers, and benzofurans. *J. Am. Chem. Soc.* **2006**, *128*, 10694–10695.
- (32) Choy, J.; Jaime-Figueroa, S.; Jiang, L.; Wagner, P. Novel practical deprotection of N-Boc compounds using fluorinated alcohols. *Synth. Commun.* **2008**, *38*, 3840–3853.
- (33) Hong, Y.; Senanayake, C. H.; Xiang, T.; Vandenbossche, C. P.; Tanoury, G. J.; Bakale, R. P.; Wald, S. A. Remarkably selective palladium-catalyzed amination process: rapid assembly of multiamino based structures. *Tetrahedron Lett.* **1998**, *39*, 3121–3124.
- (34) (a) Wolfe, J. P.; Wagaw, S.; Buchwald, S. L. An improved catalyst system for aromatic carbon–nitrogen bond formation: the possible involvement of bis(phosphine) palladium complexes as key intermediates. *J. Am. Chem. Soc.* **1996**, *118*, 7215–7216. (b) Driver, M. S.; Hartwig, J. F. A second-generation catalyst for aryl halide amination: mixed secondary amines from aryl halides and primary amines catalyzed by (DPPF)PdCl₂. *J. Am. Chem. Soc.* **1996**, *118*, 7217–7218.
- (35) (a) Darses, S.; Michaud, G.; Genêt, J. P. Potassium vinyltrifluoroborate: a stable and efficient vinylating agent of arenediazonium salts using palladium catalysts. *Tetrahedron Lett.* **1998**, *39*, 5045–5048. (b) Molander, G. A.; Rivero, M. R. Suzuki cross-coupling reactions of potassium alkenyltrifluoroborates. *Org. Lett.* **2002**, *4*, 107–109. (c) Molander, G. A.; Brown, A. R. Suzuki–Miyaura cross-coupling reactions of potassium vinyltrifluoroborate with aryl and heteroaryl electrophiles. *J. Org. Chem.* **2006**, *71*, 9681–9686.
- (36) Appel, R. Tertiary phosphane/tetrachloromethane, a versatile reagent for chlorination, dehydration, and P–N linkage. *Angew. Chem., Int. Ed. Engl.* **1975**, *14*, 801–811.
- (37) See the [Supporting Information](#) for detailed conditions.
- (38) (a) Park, N.; Park, K.; Jang, M.; Lee, S. One-pot synthesis of symmetrical and unsymmetrical aryl sulfides by Pd-catalyzed couplings of aryl halides and thioacetates. *J. Org. Chem.* **2011**, *76*, 4371–4378. (b) Wager, K. M.; Daniels, M. H. Palladium-catalyzed cross-coupling of benzyl thioacetates and aryl halides. *Org. Lett.* **2011**, *13*, 4052–4055.
- (39) Shavnya, A.; Coffey, S. B.; Smith, A. C.; Mascitti, V. Palladium-catalyzed sulfination of aryl and heteroaryl halides: direct access to sulfones and sulfonamides. *Org. Lett.* **2013**, *15*, 6226–6229.
- (40) Omura, K.; Swern, D. Oxidation of alcohols by “activated” dimethyl sulfoxide. A preparative, steric and mechanistic study. *Tetrahedron* **1978**, *34*, 1651–1660.
- (41) (a) Lindgren, B. O.; Nilsson, T. Preparation of carboxylic acids from aldehydes (including hydroxylated benzaldehydes) by oxidation with chlorite. *Acta Chem. Scand.* **1973**, *27*, 888–890. (b) Kraus, G. A.; Taschner, M. J. Model studies for the synthesis of quassinooids. 1. Construction of the BCE ring system. *J. Org. Chem.* **1980**, *45*, 1175–1176. (c) Kraus, G. A.; Roth, B. Synthetic studies toward verrucarol. 2. Synthesis of the AB ring system. *J. Org. Chem.* **1980**, *45*, 4825–4830. (d) Bal, B. S.; Childers, W. E.; Pinnick, H. W. Oxidation of α,β -unsaturated aldehydes. *Tetrahedron* **1981**, *37*, 2091–2096.
- (42) (a) Horner, L.; Hoffmann, H.; Wippel, H. G. Phosphororganische Verbindungen, XII. Phosphinoxide als olefinierungsreagenzien. *Chem. Ber.* **1958**, *91*, 61–63. (b) Horner, L.; Hoffmann, H.; Wippel, H. G.; Klahre, G. Phosphororganische Verbindungen, XX. Phosphinoxyde als olefinierungsreagenzien. *Chem. Ber.* **1959**, *92*, 2499–2505.
- (c) Wadsworth, W. S.; Emmons, W. D. The utility of phosphonate carbanions in olefin synthesis. *J. Am. Chem. Soc.* **1961**, *83*, 1733–1738.
- (43) Juszczuk, P.; Kasprzykowska, R.; Kołodziejczyk, A. S. Simple and efficient synthesis of chiral amino alcohols with an amino acid-based skeleton. *Lett. Pept. Sci.* **2003**, *10*, 79–82.
- (44) (a) Rasmussen, J. K.; Heilmann, S. M. A facile, one-pot synthesis of silylated cyanohydrins. *Synthesis* **1978**, *1978*, 219–221. (b) Gassman, P. G.; Talley, J. J. Cyanohydrins—a general synthesis. *Tetrahedron Lett.* **1978**, *19*, 3773–3776.
- (45) Thompson, A. S.; Humphrey, G. R.; DeMarco, A. M.; Mathre, D. J.; Grabowski, E. J. J. Direct conversion of activated alcohols to azides using diphenyl phosphorazidate. A practical alternative to Mitsunobu conditions. *J. Org. Chem.* **1993**, *58*, 5886–5888.
- (46) Branching off of the secondary amine, rather than the primary amine, was attempted in the phenyl series, and the analogs were found to be much less active.
- (47) Masuda, N.; Ohya, S. Cross-resistance to Meropenem, cephems, and quinolones in *Pseudomonas aeruginosa*. *Antimicrob. Agents Chemother.* **1992**, *36*, 1847–1851.
- (48) Zimmerman, W. Penetration through the gram-negative cell wall: a co-determinant of the efficacy of beta-lactam antibiotics. *Int. J. Clin. Pharmacol. Biopharm.* **1979**, *17*, 131–134.
- (49) Li, X. Z.; Zhang, L.; Srikumar, R.; Poole, K. Beta-lactamase inhibitors are substrates for the multidrug efflux pumps of *Pseudomonas aeruginosa*. *Antimicrob. Agents Chemother.* **1998**, *42*, 399–403.
- (50) Baba, T.; Ara, T.; Hasegawa, M.; Takai, Y.; Okumura, Y.; Baba, M.; Datsenko, K. A.; Tomita, M.; Wanner, B. L.; Mori, H. Construction of *Escherichia coli* K-12 in-frame, single-gene knockout mutants: the Keio collection. *Mol. Syst. Biol.* **2006**, *2* (1), 2006.0008.
- (51) Sampson, B. A.; Misra, R.; Benson, S. A. Identification and characterization of a new gene of *Escherichia coli* K-12 involved in outer membrane permeability. *Genetics* **1989**, *122*, 491–501.